

Single and double coincidence nucleon spectra in the weak decay of Λ -hypernuclei

E. Bauer¹, G. Garbarino², A. Parreño³ and A. Ramos³

¹*Departamento de Física, Universidad Nacional de La Plata,
C. C. 67, 1900 La Plata, Argentina*

²*Dipartimento di Fisica Teorica, Università di Torino and INFN, Sezione di Torino,
I-10125 Torino, Italy*

³*Departament d'Estructura i Constituents de la Matèria, Universitat de Barcelona,
E-08028 Barcelona, Spain*

(April 21, 2018)

Abstract

Recent progress has been experienced in the field of hypernuclear weak decay, especially concerning the ratio of the neutron- to proton-induced Λ non-mesonic decay rates, Γ_n/Γ_p . Theoretical analyses of nucleon coincidence data have been performed in a finite nucleus framework. They led to the extraction of Γ_n/Γ_p values in agreement with pure theoretical estimates, thus providing an evidence for the solution of a longstanding puzzle. Here we present an alternative approach to the problem, based on a nuclear matter formalism extended to finite nuclei via the local density approximation. The work is motivated by the exigence to make the determination of Γ_n/Γ_p from data less model dependent. One-meson-exchange potentials are used for describing both the one- and two-nucleon induced decays, $\Lambda N \rightarrow nN$ and $\Lambda NN \rightarrow nNN$. For the latter, treated within a microscopic approach, the channels $\Lambda nn \rightarrow nnn$ and $\Lambda pp \rightarrow npp$ are included in addition to the mode $\Lambda np \rightarrow nnp$ already considered, in a phenomenological way, in previous studies. The propagation of the final nucleons in the residual nucleus is simulated by an intranuclear cascade code. We evaluate single and double coincidence nucleon spectra for the non-mesonic decay of $^{12}\Lambda C$. Through the comparison of our predictions with KEK coincidence data we determine $\Gamma_n/\Gamma_p = 0.43 \pm 0.10$ for this hypernucleus, confirming previous finite nucleus analyses. The use of a high nucleon kinetic energy detection threshold such as 60 MeV makes the contribution of two-nucleon induced channels quite small, but final state interaction effects are still important when extracting Γ_n/Γ_p from measured single nucleon distributions. Coincidence spectra suffer less from these effects even for a moderate detection threshold such as 30 MeV. In any case, final state interactions have to be considered for meaningful determinations of Γ_n/Γ_p .

21.80.+a, 13.30.Eg, 13.75.Ev

Typeset using REVTEX

I. INTRODUCTION

Diversified efforts have been devoted to the study of hypernuclear weak decay in the latest years. Theoretical reviews on the subject can be found in Refs. [1,2] and recent, related experiments in Refs. [3–10]. Forthcoming data are expected from FINUDA [11], while new experiments are planned at J-PARC [12] and HypHI [13]. Strong evidences for a solution of the longstanding problem on the ratio Γ_n/Γ_p between the widths for the weak processes $\Lambda n \rightarrow nn$ and $\Lambda p \rightarrow np$ originated from theoretical analyses [14,15] of KEK nucleon coincidence data [7–10]. In the authors opinion, this puzzle was due to the non-trivial interpretation of experimental data, which required a careful analysis of nuclear medium effects on the weak decay nucleons, rather than to a poor understanding of the weak decay mechanism. Indeed, the lately extracted Γ_n/Γ_p values [14,15] turned out to be in agreement with the previous, pure theoretical estimates of Refs. [16–20] obtained by using one-meson-exchange potentials to describe the one-nucleon induced, $\Lambda N \rightarrow nN$ weak transitions.

Nevertheless, further theoretical and experimental work is desirable in order to confirm the previously mentioned evidence in favor of a solution of the Γ_n/Γ_p puzzle. Indeed, on the one hand such an evidence relies on particular theoretical descriptions of both the weak decay mechanism and the subsequent propagation of the produced nucleons within the residual nucleus. In this direction, the use of alternative weak decay or/and intranuclear cascade models is of interest. On the other hand, one has to consider that another problem of the field is still unsolved: it concerns the asymmetry of the protons emitted in the non-mesonic decay of polarized hypernuclei, measured to be not far from zero in recent experiments [21,22] while a large negative number is predicted by the theoretical models [17,23–26]. Recently, a strong effect of nucleon final state interactions (FSI) was pointed out [23] without, however, bringing new hints for a possible solution of the asymmetry puzzle. The connections existing among the weak decay observables [Γ_n/Γ_p , $\Gamma_{NM} = \Gamma_n + \Gamma_p + \Gamma_2$, Γ_2 being the width for two-nucleon induced decays, $\Lambda NN \rightarrow nNN$, and the asymmetry parameters] and the question concerning the validity of the $\Delta I = 1/2$ isospin rule in the non-mesonic decay is another important issue which deserves future investigations in the prospect of a better understanding of baryon–baryon weak interactions.

On the experimental side, very recent measurements of single- [3–6] and double-coincidence [7–10] nucleon spectra from the non-mesonic hypernuclear decay were reported—with accuracies largely improved with respect to the ones at disposal in previous experiments [27–31]—in forms that suggest suitable comparisons with theory. Some of these experiments have somehow managed to derive values of Γ_n/Γ_p . They are discussed in the following paragraphs.

The Γ_n/Γ_p ratio was obtained by KEK-E307 [3,4] for $^{12}\Lambda C$, $^{28}\Lambda Si$ and $^{56}\Lambda Fe$ hypernuclei from single-proton kinetic energy spectra measurements and by making use of the intranuclear cascade code of Ref. [32] (based on the polarization propagator formalism of Ref. [33]) to simulate the spectra of the nucleons emitted by the considered hypernuclei. For $^{12}\Lambda C$,

$\Gamma_n/\Gamma_p = 0.87 \pm 0.23$ ($0.60^{+0.25}_{-0.23}$) was obtained [4] by neglecting the two-nucleon induced decay mechanism (for $\Gamma_2/(\Gamma_n + \Gamma_p) = 0.35$, with $\Gamma_2 \equiv \Gamma(\Lambda np \rightarrow np)$). As the very same authors of Refs. [3,4] noted in Ref. [5], these determinations of the ratio may be affected by the fact that in the experiment the neutron-induced decay width was estimated indirectly, from the proton measurement, using the relation $\Gamma_n = \Gamma_T - \Gamma_p - \Gamma_{\pi^-} - \Gamma_{\pi^0}$, which neglects two-nucleon stimulated non-mesonic decays. This method also required the measurement of the total decay width Γ_T as well as the decay rates for the mesonic channels $\Lambda \rightarrow \pi^- p$ (Γ_{π^-}) and $\Lambda \rightarrow \pi^0 n$ (Γ_{π^0} , for which previous data from Ref. [28] were used in the analysis of Ref. [4]). Moreover, the severe energy losses suffered by protons inside the (thick) target and detector materials and the consequently high kinetic energy threshold (about 40 MeV) for proton detection in KEK-E307 did not permit an easy reconstruction of the proton spectrum emitted by the nucleus, which is essential for the indirect evaluation of Γ_n . Theoretical input about nucleon rescattering in the residual nucleus [32] was indeed necessary to supply to this problem. As a consequence, in Ref. [5] the hypothesis was advanced that Γ_n (Γ_p) might be overestimated (underestimated) in the analysis of Ref. [4] because of an underestimation in the number of emitted protons.

A controversial determination of the ratio from KEK-E369 data, based on non-demonstrated, delicate hypotheses and theoretical input (again from Ref. [32]), was reported in Ref. [5]. In this experiment, direct measurements of single-neutron kinetic energy spectra were performed (with a 10 MeV threshold) for $^{12}\Lambda$ C and $^{89}\Lambda$ Y; once analyzed together with the single-proton spectra of Refs. [3,4], a ratio $\Gamma_n/\Gamma_p = 0.51 \pm 0.15$ for $^{12}\Lambda$ C was derived by neglecting the two-nucleon induced decay channel. We shall comment on the reliability of the extraction method used for such a determination in Section III B.

To overcome the difficulties of the discussed KEK experiments, both single-neutron and single-proton energy spectra were measured simultaneously by KEK-E462 for $^5\Lambda$ He and KEK-E508 for $^{12}\Lambda$ C [6]. From these measurements, the authors concluded that $\Gamma_n/\Gamma_p \simeq (N_n/N_p - 1)/2 \simeq 0.5$ for both $^5\Lambda$ He and $^{12}\Lambda$ C, N_n (N_p) being the total number of neutrons (protons) with kinetic energies T_N above 60 MeV. However, one has to note that the previous approximate relation between Γ_n/Γ_p and N_n/N_p is only valid when FSI and two-nucleon induced decay effects can be neglected. The predictions of Ref. [15] and the results presented in Sections III A and III B prove that FSI are not negligible even when a high detection threshold such as $T_N^{\text{th}} = 60$ MeV is used.

In the experiments KEK-E462 ($^5\Lambda$ He) and KEK-E508 ($^{12}\Lambda$ C), nucleon-nucleon coincidence spectra were also measured [7–10]. Quite clean angular and energy correlations between neutron-neutron and neutron-proton emitted pairs (i.e., back-to-back kinematics and $T_{N_1} + T_{N_2} \simeq 155$ MeV) were observed, thus representing the first direct experimental evidence of the existence of the two-body decays $\Lambda n \rightarrow nn$ and $\Lambda p \rightarrow np$. The ratio, N_{nn}/N_{np} , between the numbers of emitted neutron-neutron and neutron-proton pairs was measured to be around 0.5 for both $^5\Lambda$ He and $^{12}\Lambda$ C after applying the angular and energy restrictions: $\cos \theta_{NN} \leq -0.8$ and $T_N \geq 30$ MeV. The authors of Ref. [8,9] concluded that, under these

constraints, $\Gamma_n/\Gamma_p \simeq N_{nn}/N_{np} \simeq 0.5$ on the basis of a supposed cancellation of FSI and two-nucleon stimulated decays effects. In a very recent work [10], the result $\Gamma_n/\Gamma_p = 0.51 \pm 0.13 \pm 0.04$ was deduced by the KEK collaboration for ${}^{\Lambda}{}_{\Lambda}{}^{12}\text{C}$ after correcting for FSI effects by making use of the number of detected proton-proton pairs in addition to measurements of N_{nn} and N_{np} . A rather schematic method, not completely reliable in our opinion, quite in line with the one used in Ref. [5], was applied to determine Γ_n/Γ_p . We shall discuss the effect of FSI and two-nucleon induced decays in the extraction of Γ_n/Γ_p from measurements of N_{nn}/N_{np} in Section III E.

Despite this recent experimental progress, improved and/or independent measurements are awaited for a really complete understanding of the $\Lambda N \rightarrow nN$ reaction in nuclei. On this respect, the observation of the weak decay of neutron and proton rich hypernuclei [11,13] would also be source of new information.

On the theoretical side, Refs. [14,15] presented an extensive study of single- and double-coincidence nucleon spectra for the non-mesonic decay of ${}^5\Lambda\text{He}$ and ${}^{\Lambda}{}_{\Lambda}{}^{12}\text{C}$ hypernuclei. A one-meson-exchange (OME) model was used for the $\Lambda N \rightarrow nN$ transition in a finite nucleus framework. The two-nucleon induced decay channel $\Lambda np \rightarrow nnp$ was taken into account via the polarization propagator method in the local density approximation of Refs. [33,34]. The intranuclear cascade code of Ref. [32] was used to simulate the nucleon propagation inside the residual nucleus. Comparison with KEK-E462 and KEK-E508 coincidence data [7–9] lead to the determination of Γ_n/Γ_p values around 0.3-0.4 for both ${}^5\Lambda\text{He}$ and ${}^{\Lambda}{}_{\Lambda}{}^{12}\text{C}$. The relationship between Γ_n/Γ_p and the observable ratio between neutron-neutron and neutron-proton pairs, N_{nn}/N_{np} , was established for the first time in Ref. [15]. It was shown that FSI and two-nucleon induced decays significantly affect the extraction of Γ_n/Γ_p from coincidence data even when favorable energy and angular correlation restrictions are imposed on the observed nucleon pairs. Coincidence measurements of course make the determination of Γ_n/Γ_p easier and cleaner, since FSI and two-nucleon induced decay effects are reduced with respect to the ones emerging in analyses of single nucleon observables such as N_n/N_p . Nevertheless, contrary to what claimed in Refs. [7–9], they do not permit an exclusive identification of the non-mesonic decay channels as neutron- and proton-induced. Thus, $\Gamma_n/\Gamma_p \neq N_{nn}/N_{np}$ (see figures 11 and 12 of Ref. [15] and the present discussion in Section III E), indicating that to determine Γ_n/Γ_p one has to rely on experimental as well as theoretical coincidence spectra.

With the purpose of making the extraction of Γ_n/Γ_p less model dependent, in the present paper we make use of an alternative framework for hypernuclear decay: it consists of a nuclear matter formalism [19,20] extended to finite nuclei via the local density approximation, with the same weak OME transition potential (containing π , ρ , K , K^* , ω and η exchange) of Ref. [17], in addition to the Monte Carlo intranuclear cascade code of Ref. [32]. At variance with previous analyses, in the present paper we follow a microscopic approach for the two-nucleon induced decay, also including the channels $\Lambda nn \rightarrow nnn$ and $\Lambda pp \rightarrow npp$ besides the standard mode $\Lambda np \rightarrow nnp$. Most of the results shown are for the intermediate-mass hypernucleus ${}^{\Lambda}{}_{\Lambda}{}^{12}\text{C}$, but we also present some results for a heavier hypernucleus, ${}^{\Lambda}{}_{\Lambda}{}^{89}\text{Y}$. Both

cases can be well described within a local density approximation.

The paper is organized in the following way. The weak decay models employed in the calculation are outlined in Section II A. In Section II B we give a few details of the intranuclear cascade simulation. Numerical results for single and double coincidence nucleon distributions are presented and compared with data in Section III. The contribution of the two-nucleon induced decay channels is analyzed with special regard. Finally, in Section IV we draw our conclusions.

II. MODELS

A. Weak decay

The weak decay transitions as well as the distributions of the weak decay nucleons are obtained by means of a many-body description of the Λ self-energy in nuclear matter, based on the polarization propagator method (PPM) originally proposed by Oset and Salcedo [35]. The local density approximation (LDA) is employed to extend the calculation to finite nuclei. This approach was previously established [19,20] to evaluate the non-mesonic decay widths of $^{12}\Lambda\text{C}$. There is a major value of this model which by itself adds sufficient novelty to the present work with respect to previous analyses [14,15] of the nucleon spectra from hypernuclear non-mesonic decay. We must indeed emphasize that the present approach is more microscopic (i.e., less phenomenological) than the previous ones. Indeed, in addition to the generally considered $\Lambda np \rightarrow nnp$ channel, also the $\Lambda nn \rightarrow nnn$ and $\Lambda pp \rightarrow npp$ mechanisms are now evaluated. The present approach is then more in line with the functional approach—in the framework of the bosonic loop expansion—used in Ref. [36], with the difference that a clear separation into one- and two-nucleon induced channels is now possible.

1. One-nucleon induced decay

We start with a brief summary concerning the evaluation of the one-nucleon ($1N$) induced decay widths Γ_n and Γ_p . Details can be found in Refs. [19,35]. It is convenient to work first with the partial decay width $\Gamma_{t_\Lambda t_N \rightarrow t_{N'} t_{N''}}(p_\Lambda, k_F)$, where p_Λ is the Λ energy-momentum, k_F is the Fermi momentum of nuclear matter and the t_i 's represent the isospin projections of the baryons. Using the standard Goldstone rules for diagrams in nuclear matter, it is straightforward to write for the partial decay width:

$$\begin{aligned} \Gamma_{t_\Lambda t_{h2} \rightarrow t_{p1} t_{p2}}(p_\Lambda, k_F) &= -2 \text{Im} \int \frac{d^4 q}{(2\pi)^4} \int \frac{d^4 p_2}{(2\pi)^4} G_{\text{part}}(p_\Lambda - q) G_{\text{part}}(p_2) G_{\text{hole}}(p_2 - q) \\ &\quad \times \frac{1}{4} \sum \left(\left| \langle \gamma_{p1} \gamma_{p2} | V^{\Lambda N \rightarrow n N}(q) | \gamma_\Lambda \gamma_{h2} \rangle \right|^2 \right. \\ &\quad \left. - \langle \gamma_{p1} \gamma_{p2} | V^{\Lambda N \rightarrow n N}(q) | \gamma_\Lambda \gamma_{h2} \rangle^* \langle \gamma_{p2} \gamma_{p1} | V^{\Lambda N \rightarrow n N}(p_\Lambda - p_2) | \gamma_\Lambda \gamma_{h2} \rangle \right), \end{aligned} \quad (2.1)$$

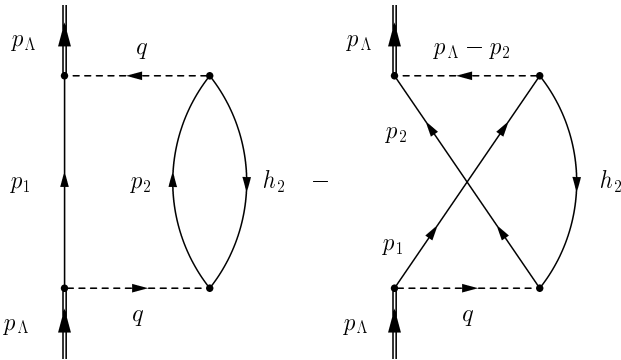


FIG. 1. Direct and exchange Λ self-energy diagrams corresponding to the one-nucleon induced decay channel in nuclear matter.

where p_i (h_i) stands for the energy-momentum of particles (holes). The meaning of each p_i and h_i is shown in Fig. 1, where we have drawn the Λ self-energy diagrams from which the relevant transition amplitude is obtained. From the energy-momentum conservation in each vertex we have $p_1 = p_\Lambda - q$ and $h_2 = p_2 - q$. For simplicity, γ_i represents the spin and isospin projections of particle i . The one-meson-exchange weak transition potential, $V^{\Lambda N \rightarrow nN}$, takes into account the complete pseudoscalar and vector meson octets ($\pi, \eta, K, \rho, \omega, K^*$) through the parameterization of Ref. [17]. The summation in Eq. (2.1) runs over all spins and isospins of the weak transition potential. Note that the first term in the *r.h.s.* of this equation is the usually called direct contribution, while the second one is the exchange term.

The particle and hole propagators are, respectively:

$$G_{\text{part}}(p) = \frac{\theta(|\mathbf{p}| - k_F)}{p_0 - E_N(\mathbf{p}) - V_N + i\varepsilon}, \quad (2.2)$$

$$G_{\text{hole}}(h) = \frac{\theta(k_F - |\mathbf{h}|)}{h_0 - E_N(\mathbf{h}) - V_N - i\varepsilon},$$

where $E_N(\mathbf{p}) = m_N + \mathbf{p}^2/2m_N$ is the nucleon total free energy and V_N the nucleon binding energy.

By integrating Eq. (2.1) over \mathbf{p}_Λ one obtains the k_F -dependent width:

$$\Gamma_{t_\Lambda t_{h2} \rightarrow t_{p1} t_{p2}}(k_F) = \int d\mathbf{p}_\Lambda \Gamma_{t_\Lambda t_{h2} \rightarrow t_{p1} t_{p2}}(p_\Lambda, k_F) |\psi_\Lambda(\mathbf{p}_\Lambda)|^2, \quad (2.3)$$

where for the Λ wave-function, $\psi_\Lambda(\mathbf{p}_\Lambda)$, we take the $1s_{1/2}$ wave-function of a harmonic oscillator and the Λ energy, $(p_\Lambda)_0$, is taken as $(p_\Lambda)_0 = m_\Lambda + \mathbf{p}_\Lambda^2/2m_\Lambda + V_\Lambda$, where V_Λ is the experimental Λ binding energy. To evaluate the decay width for a particular nucleus, one uses either an effective Fermi momentum or the LDA [35]. In the last case, k_F is spatially dependent and the transition rate reads

$$\Gamma_{t_\Lambda t_{h2} \rightarrow t_{p1} t_{p2}} = \int d\mathbf{r} \Gamma_{t_\Lambda t_{h2} \rightarrow t_{p1} t_{p2}}(k_F(r)) |\tilde{\psi}_\Lambda(\mathbf{r})|^2, \quad (2.4)$$

where $\tilde{\psi}_\Lambda(\mathbf{r})$ is the Fourier transform of $\psi_\Lambda(\mathbf{p}_\Lambda)$.

Finally, by summing up over the isospin of baryons one obtains:

$$\begin{aligned}\Gamma_n &\equiv \Gamma_{\Lambda n \rightarrow nn}, \\ \Gamma_p &\equiv \Gamma_{\Lambda p \rightarrow np} + \Gamma_{\Lambda p \rightarrow pn},\end{aligned}\tag{2.5}$$

and the $1N$ –induced decay width is:

$$\Gamma_1 = \Gamma_n + \Gamma_p.\tag{2.6}$$

We have to stress that exchange terms are very important for an accurate evaluation of Γ_1 [19]. The present work calculates exactly the exchange terms in nuclear matter. The Random Phase Approximation (RPA) corrections have not been taken into account, because a precise evaluation of RPA–exchange terms is a rather involved task, which goes beyond the scope of the present contribution.

At this point we have to mention that the models of Refs. [17,19,20] have been recently improved. On the one hand, a more realistic Λ wave–function, obtained in terms of the experimental hyperon binding energy, has been considered in the LDA calculation of Refs. [19,20], leading to a reduction of about 25% on the $1N$ –induced decay rates, Γ_n and Γ_p , and of 30-40% on the $2N$ –induced ones, Γ_{nn} , Γ_{np} and Γ_{pp} , with respect to the original results. On the other hand, a numerically more accurate evaluation of the distorted final state wave–functions has been implemented in the finite nucleus approach of Ref. [17] and the rates increase by about 15%. In both cases the ratio Γ_n/Γ_p is essentially left unchanged. The updated predictions, used in the present work, are given in Table I. Fortunately, the spectra discussed in Refs. [14,15], being normalized per non–mesonic weak decay, are not affected by the corrections of Ref. [17]. Note that the non–mesonic rate Γ_{NM} of the finite nucleus calculation is underestimated by about 25% because it lacks the contribution of the $2N$ –stimulated mechanism. On the other hand, the LDA result is overestimated because two–body final state interactions between the emitted nucleons were not considered. As shown in Ref. [17], the omission of this effect leads to rates larger by as much as a factor of two. However, this factor disappears in the normalized spectra discussed in the present work and used for the important purpose of extracting Γ_n/Γ_p from measured distributions.

For a comparison with experiment, in Table I we also report data for Γ_{NM} and Γ_n/Γ_p . Only experimental determinations of Γ_n/Γ_p obtained from single–nucleon measurements are quoted. Large experimental errors affect all but the most recent data, especially for Γ_n/Γ_p . Almost all Γ_n/Γ_p data appear to strongly overestimate any theoretical prediction found in the literature.

2. Two–nucleon induced decay

In the quasi–deuteron approximation, the $2N$ –induced decay mode turns out to be dominated by the process $\Lambda np \rightarrow nn p$: the meson emitted in the Λ vertex is mainly absorbed

TABLE I. Non-mesonic weak decay rates (in units of the free Λ decay width) predicted for ^{12}C by the updated finite nucleus approach (OMEa and OMEf calculations) of Ref. [17] and LDA model of Refs. [19,20].

Ref.	Γ_n	Γ_p	Γ_{nn}	Γ_{np}	Γ_{pp}	Γ_n/Γ_p	Γ_{NM}
Finite Nucleus, OMEa	0.190	0.625				0.303	0.815
Finite Nucleus, OMEf	0.173	0.484				0.356	0.657
LDA	0.267	0.936	0.017	0.238	0.062	0.285	1.521
KEK-E508 [8]							0.953 ± 0.032
KEK-E369 [5]						0.51 ± 0.15	
KEK-E307 [4]						$0.87 \pm 0.09 \pm 0.21$	$0.828 \pm 0.056 \pm 0.066$
KEK [30]						$1.87 \pm 0.59^{+0.32}_{-1.00}$	$0.89 \pm 0.15 \pm 0.03$
BNL [29]						$1.33^{+1.12}_{-0.81}$	1.14 ± 0.20

by an isoscalar neutron–proton correlated pair. However, the isospin quantum number also allows two others mechanisms, $\Lambda nn \rightarrow nnn$ and $\Lambda pp \rightarrow npp$, which then contribute to the decay rate Γ_2 . Here we briefly outline our main expressions needed for the evaluation of this rate, which include all the just mentioned processes within a nuclear matter framework. A complete description of this decay channel can be found in Ref. [20].

At variance with Γ_1 , we limit ourselves to direct terms. This is because Γ_2 is originated from ground state correlations (GSC). It was shown in Ref. [37] that, in the case of electron scattering, the exchange terms for the two particle–two hole polarization propagator can be neglected. In fact, in that work it was concluded that exchange terms are not relevant in the graphs originated from GSC.

Furthermore, it is a good approximation [38] to consider only contributions where the two weak transition potentials $V^{\Lambda N \rightarrow nN}$ (which again include the exchange of π , ρ , K , K^* , η and ω mesons [17]) of the Λ self-energy are attached to the same bubble. There are thus three different self-energy contributions, which we denote by pp, ph and hh. In the first one, the two $V^{\Lambda N \rightarrow nN}$ are attached to the same particle (see Fig. 2). In the ph contribution one $V^{\Lambda N \rightarrow nN}$ is connected to a particle and the other one to a hole. Finally, the two potentials are attached to the same hole for the hh part. To illustrate the method, we present the pp contribution to Γ_2 . From Goldstone rules, the pp–partial decay width is:

$$\begin{aligned} \Gamma_{t_\Lambda t_{h2} t_{h3} \rightarrow t_{p1} t_{p2} t_{p3}}^{\text{pp}}(p_\Lambda, k_F) = & -2 \text{Im} \int \frac{d^4 p_2}{(2\pi)^4} \int \frac{d^4 p_3}{(2\pi)^4} \int \frac{d^4 q}{(2\pi)^4} \int \frac{d^4 q'}{(2\pi)^4} & (2.7) \\ & \times \frac{1}{8} \sum G_{\text{part}}(p_\Lambda - q) G_{\text{part}}(p_2) G_{\text{part}}^2(p_2 - q) G_{\text{part}}(p_3) \\ & \times G_{\text{hole}}(p_2 - q + q') G_{\text{hole}}(p_3 - q') \\ & \times \left| \langle \gamma_{p1} \gamma_{p2} | V^{\Lambda N \rightarrow nN}(q) | \gamma_\Lambda \gamma_{p'2} \rangle \right|^2 \left| \langle \gamma_{p'2} \gamma_{p3} | V^{NN}(q') | \gamma_{h2} \gamma_{h3} \rangle \right|^2. \end{aligned}$$

The meaning of each energy–momentum p_i and h_i is shown in Fig. 2. From energy–

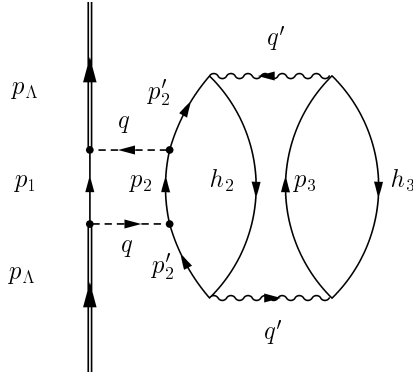


FIG. 2. pp–part of the two particle–two hole contribution to the Λ self–energy in nuclear matter.

momentum conservation in each vertex we have: $p_1 = p_\Lambda - q$, $p'_2 = p_2 - q$, $h_2 = p_2 - q + q'$ and $h_3 = p_3 - q'$. Again, γ_i stands for the spin and isospin projections of particle i . The nuclear residual interaction V^{NN} is modeled by a Bonn potential [39] in the framework of the parameterization presented in Ref. [40], which contains the exchange of π , ρ , σ and ω mesons and neglects the small η and δ –mesons contributions. The summation in Eq. (2.7) runs over all spins and over $t_{p'_2}$.

After performing the LDA as described in the previous subsection, the summation over the isospin of baryons leads to:

$$\begin{aligned}\Gamma_{nn}^{\text{pp}} &\equiv \Gamma_{\Lambda nn \rightarrow nnn}^{\text{pp}}, \\ \Gamma_{np}^{\text{pp}} &\equiv \Gamma_{\Lambda np \rightarrow nnp}^{\text{pp}} + \Gamma_{\Lambda pn \rightarrow nnp}^{\text{pp}} + \Gamma_{\Lambda np \rightarrow npn}^{\text{pp}} + \Gamma_{\Lambda pn \rightarrow npn}^{\text{pp}} + \Gamma_{\Lambda np \rightarrow pnn}^{\text{pp}} + \Gamma_{\Lambda pn \rightarrow pnn}^{\text{pp}}, \\ \Gamma_{pp}^{\text{pp}} &\equiv \Gamma_{\Lambda pp \rightarrow npp}^{\text{pp}} + \Gamma_{\Lambda pp \rightarrow npn}^{\text{pp}}.\end{aligned}\quad (2.8)$$

Thus, once the ph and hh channels are included, the $2N$ –induced decay width is obtained as:

$$\Gamma_2 = \Gamma_{nn} + \Gamma_{np} + \Gamma_{pp}, \quad (2.9)$$

where ($ij = nn$, np or pp):

$$\Gamma_{ij} = \Gamma_{ij}^{\text{pp}} + \Gamma_{ij}^{\text{ph}} + \Gamma_{ij}^{\text{hh}}. \quad (2.10)$$

Explicit expressions for all contributions can be found in Ref. [20].

The results obtained for the $2N$ –stimulated decay widths are given in Table I. As expected, the dominant contribution to Γ_2 originates from the np –induced decay, $\Lambda np \rightarrow nnp$. Nevertheless, the other $2N$ –induced channels cannot be neglected. The prediction $\Gamma_2/\Gamma_1 = 0.26$ is in agreement with the phenomenological estimate $\Gamma_2/\Gamma_1 = 0.25$ of Refs. [14,15].

B. Intranuclear cascade

After the Λ interacts with one (two) nucleons, the two (three) produced nucleons will interact with other nucleons in their way out of the nucleus. This process, which will generate secondary nucleons, is accounted for by the intranuclear cascade model described in Ref. [32]. This model considers a semiclassical propagation of primary (i.e., weak decay) and secondary nucleons. Nucleons move along classical, straight trajectories between collision points and under the influence of a local (i.e., R -dependent) mean potential, $V_N(R) = -k_{F_N}(R)^2/2m_N$, where $k_{F_N}(R) = [3\pi^2\rho_N(R)]^{1/3}$ is the local nucleon ($N = n, p$) Fermi momentum corresponding to the nucleon density $\rho_N(R)$. Propagating nucleons also collide with the nucleons of the medium according to free space nucleon–nucleon cross sections properly corrected to take into account the Pauli blocking and Fermi motion effects. For more details of the code we refer to Ref. [32].

The description in terms of semiclassical nucleon propagation is justified when the nucleon wavelength λ is much smaller than the average distance between nucleons, d , and the range of the nucleon–nucleon interaction, r_0 : $\lambda \ll r_0 \leq d$ [41]. For a 30 MeV kinetic energy nucleon, $\lambda = 0.8$ fm, which has to be compared with $d \simeq 2$ fm in $^{12}\Lambda$ C and $r_0 \simeq 1.4$ fm. The spectra for nucleon kinetic energies $\lesssim 30$ MeV could thus show unrealistic behaviors. For this reason, all the comparison with data will intervene by introducing a kinetic energy cut of at least 30 MeV.

III. RESULTS

A. Single–nucleon spectra

In Figure 3 a comparison is shown between the present LDA calculation and the previous finite nucleus evaluation of Refs. [14,15]. The number of primary protons emitted in the $1N$ –induced non–mesonic weak decay of $^{12}\Lambda$ C is given as a function of the proton kinetic energy. In order to make the comparison model independent, the spectra are normalized per $1N$ –induced decay assuming $\Gamma_n/\Gamma_p = (\Gamma_n/\Gamma_p)^{\text{LDA}} = 0.285$, which is equivalent to normalize per the corresponding proton–induced decay rate. We observe that the Full Width a Half Maximum (FWHM) of the LDA distribution is 15–20 MeV larger than the one of the finite nucleus spectrum. This is essentially due to the more pronounced Fermi motion effects in the nuclear matter calculation. Consistently with this expectation, in the finite nucleus calculation of Refs. [14,15] we found that the primary nucleon distributions for $^{12}\Lambda$ C were slightly broader than the ones for ^5He .

In Figure 4 we show the single–proton kinetic energy spectra for the non–mesonic weak decay of $^{12}\Lambda$ C once $2N$ –induced decays and FSI effects are included. All spectra are normalized per non–mesonic weak decay. The continuous line refers to the present LDA result. The dashed line has been obtained with the LDA of Ref. [32], where the weak transition potential was described by a correlated pion exchange. The old LDA spectrum corresponds to the

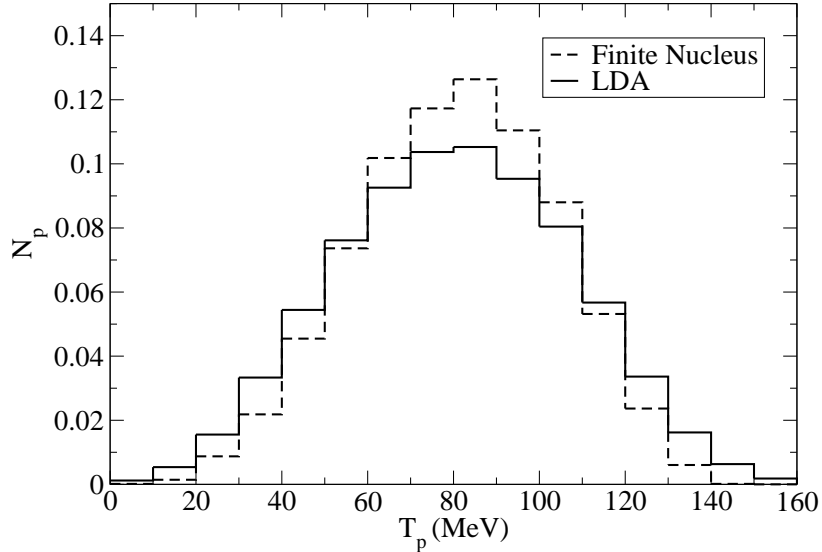


FIG. 3. Kinetic energy spectra of primary protons from the $1N$ –induced non–mesonic weak decay of $^{12}\Lambda C$. The continuous line refers to the present LDA calculation, the dashed one to the finite nucleus evaluation of Refs. [14,15]. Both curves are normalized per $1N$ –induced decay assuming $\Gamma_n/\Gamma_p = (\Gamma_n/\Gamma_p)^{\text{LDA}} = 0.285$.

same Γ_n/Γ_p of the present LDA, $\Gamma_n/\Gamma_p = (\Gamma_n/\Gamma_p)^{\text{LDA}} = 0.285$. Good agreement is obtained between the two LDA calculations despite the different weak decay models employed. The dot–dashed line has been taken from the finite nucleus evaluation of Refs. [14,15] fixing $\Gamma_n/\Gamma_p = (\Gamma_n/\Gamma_p)^{\text{LDA}} = 0.285$. Again, the differences between LDA and finite nucleus estimates are mainly due to the different phase spaces in the two cases. As it is apparent from Figure 4, all the theoretical spectra are in strong disagreement with KEK–E508 data [6]. Not even a calculation enforcing a large value of Γ_n/Γ_p such as 1 in the old LDA (dotted curve) is able to reproduce the data. Surprisingly, such a LDA [32] was able to reproduce the KEK–E307 single–proton data of Ref. [4] with values of Γ_n/Γ_p smaller than 1, as reported in the Introduction. This indicates that the two sets of data are inconsistent with each other. A clarification of this discrepancy would be desirable.

In contrast, the single–neutron spectrum measured by KEK–E508 [6] is compatible, within error bars, with the previous distribution measured by the KEK–E369 experiment [5], as can be seen in Fig. 5. Here, results of the present LDA calculation are also shown, both for the primary neutrons coming from the $1N$ –induced mechanism (dashed line) and after including $2N$ –induced decays and FSI effects (solid line). The full result is in good agreement with both sets of data.

We note in passing that a model having a sufficiently large value of Γ_n/Γ_p to reproduce the KEK–E508 proton spectrum of Fig. 4 would inevitably overestimate the neutron spectra of KEK–E508 and KEK–E369 shown in Fig. 5. We would also like to point out that the KEK–E508 proton spectrum of Fig. 4 have suffered a much stronger correction from energy

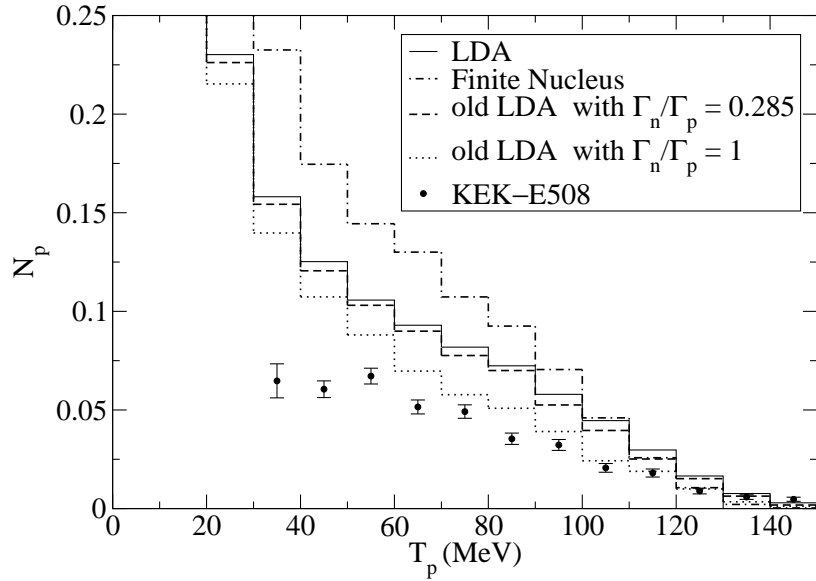


FIG. 4. Single-proton kinetic energy spectra for the non-mesonic weak decay of $^{12}\Lambda$ C after $2N$ -induced decays and FSI effects are included. Data are from KEK-E508 [6]. All results are normalized per non-mesonic weak decay. See detailed explanation in the text.

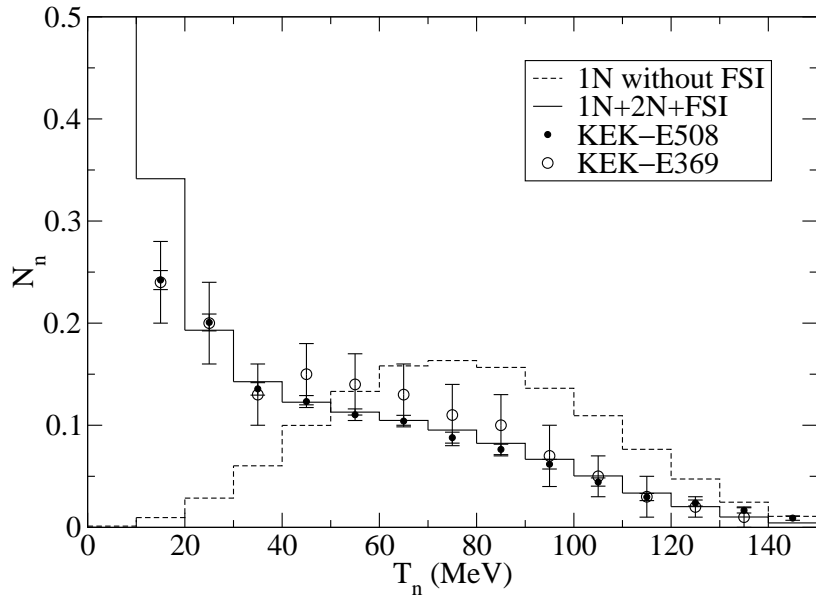


FIG. 5. Single-neutron kinetic energy spectra for the non-mesonic weak decay of $^{12}\Lambda$ C. The dashed line corresponds to the distribution of primary neutrons, while the continuous line is obtained once $2N$ -induced decays and FSI effects are included. Data are from KEK-E369 [5] and KEK-E508 [6]. The spectrum of primary neutrons (experimental data and the full theoretical result) is (are) normalized per $1N$ -induced (total) non-mesonic weak decay.

losses in target and detector materials than the neutron spectra of Fig. 5.

We would like to comment now on a disagreement between theory and experiment concerning the decay of ${}^5_{\Lambda}\text{He}$. The calculation of Ref. [15] predicted a quite pronounced peak at $T_n \simeq 75$ MeV in the single-neutron energy spectra from ${}^5_{\Lambda}\text{He}$ non-mesonic decay. Even if a LDA formalism is not the best description for this light hypernucleus, we have checked that a very similar peak is also produced by the present model. In contrast, almost no peaking structure was found in the KEK-E462 experiment of Ref. [6].

To gain some insight into this discrepancy, we put forward a simple theoretical argument that shows that single-*neutron* spectra are expected to be less influenced by FSI than single-*proton* spectra. In this discussion we safely neglect $2N$ -stimulated decays. We start by noting that, for any value of Γ_n/Γ_p , the number of primary neutrons is larger than that of primary protons, i.e., $N_n^{\text{wd}}/N_p^{\text{wd}} = 2\Gamma_n/\Gamma_p + 1$ is always larger than 1. Consequently, due to $np \rightarrow np$ reactions, the proportion of secondary protons in the proton spectrum N_p (mainly at low kinetic energies) is larger than the proportion of secondary neutrons in the neutron spectrum N_n . Note that $nn \rightarrow nn$ and $pp \rightarrow pp$ reactions, occurring with almost identical cross sections, produce the same proportion of secondary neutrons in N_n and secondary protons in N_p , respectively. For this reason, our maxima at $T_N \simeq 75$ MeV for ${}^5_{\Lambda}\text{He}$ are more evident for neutrons than for protons (compare Fig. 3 and 4 of Ref. [15]). Due to stronger FSI, such maxima completely disappear for ${}^{12}_{\Lambda}\text{C}$ (compare Fig. 5 and 6 of Ref. [15]), but again protons are more affected by FSI than neutrons.

According to this discussion, a similar shape of neutron and proton spectra—as indicated by the experiment of Ref. [6] for ${}^{12}_{\Lambda}\text{C}$ —is only possible for $N_n^{\text{wd}} \simeq N_p^{\text{wd}}$ and thus for small values of Γ_n/Γ_p . For $\Gamma_n/\Gamma_p = 0$ we predict $N_n \simeq N_p$ (see Fig. 7), but KEK obtained $N_n/N_p \simeq 2$ for both ${}^5_{\Lambda}\text{He}$ and ${}^{12}_{\Lambda}\text{C}$. The similar neutron and proton KEK-E462 spectral shapes thus look surprising.

Another point raised in the Conclusion of Ref. [6] has to be commented. There, Okada et al. claim that the observed single-neutron spectrum from ${}^5_{\Lambda}\text{He}$ “indicates the importance of the multi-nucleon induced process in the non-mesonic weak decay or/and a large FSI effect”. Here we want to emphasize that only a very large and quite certainly unrealistic proportion of $2N$ -stimulated decays could eliminate the maximum that we found at $T_n \simeq 75$ MeV for ${}^5_{\Lambda}\text{He}$ decay. Besides, the disappearance of this maximum would require a too strong amount of FSI.

In Fig. 6 we show the single-neutron energy spectrum obtained for the non-mesonic decay of ${}^{89}_{\Lambda}\text{Y}$. This result is compared with the distribution obtained by the experiment KEK-E369 [5]. The quite good agreement between theory and data for a hypernucleus as heavy as ${}^{89}_{\Lambda}\text{Y}$ is an indicator of the reliability in using the intranuclear cascade code of Ref. [32] to simulate the nucleon FSI in hypernuclear decay.

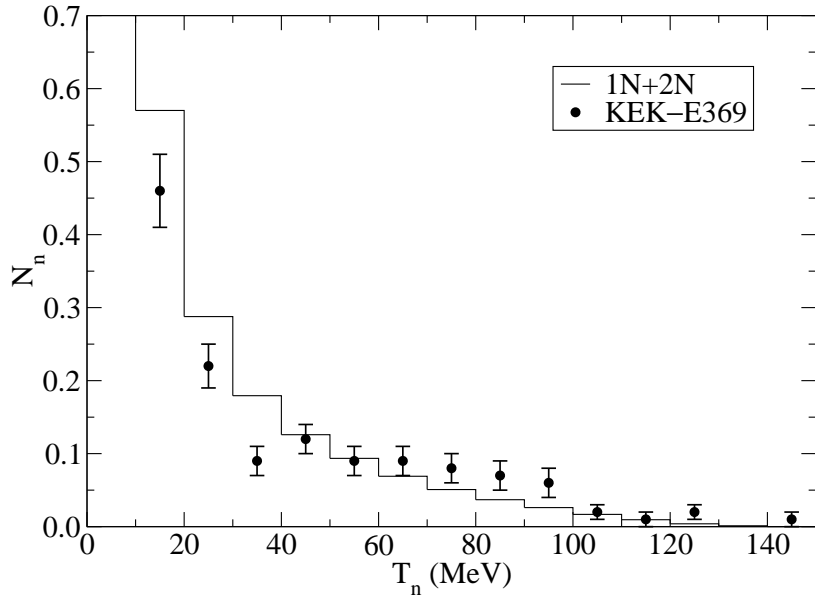


FIG. 6. Single-neutron kinetic energy spectra for the non-mesonic weak decay of $^{89}\Lambda$ -Y. Data are from KEK-E369 [5]. All results are normalized per non-mesonic weak decay.

B. Ratio N_n/N_p

We would like to compare now our results for the ratio between the number of neutrons and the number of protons produced in the decay of $^{12}\Lambda$ -C with experimental observations. Since our definitive aim is to determine Γ_n/Γ_p by such a comparison, it is convenient [15] to start by introducing the number of nucleons of type N ($N = n$ or p) produced in n -induced (N_N^{1Bn}), p -induced (N_N^{1Bp}), nn -induced (N_N^{2Bnn}), np -induced (N_N^{2Bnp}) and pp -induced (N_N^{2Bpp}) decays. By normalizing these quantities per n -, p -, nn -, np - and pp -induced decay, respectively, the total number of nucleons of the type N normalized per non-mesonic weak decay is given by:

$$N_N = \frac{N_N^{1Bn}\Gamma_n + N_N^{1Bp}\Gamma_p + N_N^{2Bnn}\Gamma_{nn} + N_N^{2Bnp}\Gamma_{np} + N_N^{2Bpp}\Gamma_{pp}}{\Gamma_n + \Gamma_p + \Gamma_{nn} + \Gamma_{np} + \Gamma_{pp}}. \quad (3.1)$$

By definition, the nucleon numbers N_N^{1Bn} , N_N^{1Bp} , etc, are independent of the model employed to describe the weak decay. Their values depend on the strong interaction part of the problem, related to nucleon FSI, and on the framework (finite nucleus or nuclear matter) used for treating the hypernuclear structure effects, which produce different phase space factors. The dependence on the weak decay model enters Eq. (3.1) via the various partial decay widths.

In table II we report our results for the weak decay model independent nucleon numbers in the case of a kinetic energy threshold for nucleon detection of $T_N^{\text{th}} = 60$ MeV. From Eq. (3.1) and our results of Tables I and II we then determine:

TABLE II. Predictions for the weak interaction model independent quantities $N_N^{1\text{Bn}}$, $N_N^{1\text{Bp}}$, $N_N^{2\text{Bnn}}$, $N_N^{2\text{Bnp}}$, $N_N^{2\text{Bpp}}$ and for $N_N^{2\text{B}}$ of Eqs. (3.1) and (3.4)–(3.6) for $^{12}\Lambda\text{C}$ and nucleon kinetic energies $T_N \geq 60$ MeV.

$N_n^{1\text{Bn}}$	$N_n^{1\text{Bp}}$	$N_n^{2\text{Bnn}}$	$N_n^{2\text{Bnp}}$	$N_n^{2\text{Bpp}}$	$N_n^{2\text{B}}$
0.91	0.47	0.67	0.50	0.17	0.45
$N_p^{1\text{Bn}}$	$N_p^{1\text{Bp}}$	$N_p^{2\text{Bnn}}$	$N_p^{2\text{Bnp}}$	$N_p^{2\text{Bpp}}$	$N_p^{2\text{B}}$
0.11	0.54	0.08	0.21	0.56	0.27

$$\frac{N_n}{N_p} = 1.33. \quad (3.2)$$

We have to note that this result is close to the ones obtained in the finite nucleus calculation of Ref. [15], namely $N_n/N_p = 1.38$ and 1.42 , using the OMEa and OMEf model, respectively. If the $2N$ –stimulated decay mode is neglected, the present calculation predicts

$$\left(\frac{N_n}{N_p} \right)^{1\text{N}} = 1.28. \quad (3.3)$$

These results underestimate the value $N_n/N_p = 2.00 \pm 0.17$ obtained by KEK–E508 [6] for $T_N^{\text{th}} = 60$ MeV. Such an occurrence is related to the disagreement between theory and experiment for the single–proton spectra of Fig. 4. Our results of Eqs. (3.2) and (3.3) should also be compared with the previous experimental determination, $N_n/N_p = 1.73 \pm 0.22$, obtained from KEK–E369 and KEK–E307 data [5] and for a detection threshold of about 40 MeV.

It is interesting to mention that, on the contrary, for $^{5}\Lambda\text{He}$, KEK–E462 [6] measured $N_n/N_p = 2.17 \pm 0.22$, which fairly agrees with the values obtained in Ref. [15], namely $N_n/N_p = 1.78$ and 1.98 for the OMEa and OMEf models, respectively.

In order to determine Γ_n/Γ_p for $^{12}\Lambda\text{C}$, we now consider a weak decay model independent analysis of the mentioned KEK–E508 data. From Eq. (3.1) written for neutrons and protons one obtains:

$$\frac{N_n}{N_p} = \frac{N_n^{1\text{Bn}} \frac{\Gamma_n}{\Gamma_p} + N_n^{1\text{Bp}} + \frac{1}{\Gamma_1} \left(1 + \frac{\Gamma_n}{\Gamma_p} \right) \left(N_n^{2\text{Bnn}} \Gamma_{nn} + N_n^{2\text{Bnp}} \Gamma_{np} + N_n^{2\text{Bpp}} \Gamma_{pp} \right)}{N_p^{1\text{Bn}} \frac{\Gamma_n}{\Gamma_p} + N_p^{1\text{Bp}} + \frac{1}{\Gamma_1} \left(1 + \frac{\Gamma_n}{\Gamma_p} \right) \left(N_p^{2\text{Bnn}} \Gamma_{nn} + N_p^{2\text{Bnp}} \Gamma_{np} + N_p^{2\text{Bpp}} \Gamma_{pp} \right)}. \quad (3.4)$$

The ratio Γ_n/Γ_p is thus obtained in terms of our theoretical values for Γ_{nn}/Γ_1 , Γ_{np}/Γ_1 and Γ_{pp}/Γ_1 and from data for N_n/N_p as:

$$\frac{\Gamma_n}{\Gamma_p} = \frac{N_n^{1\text{Bp}} + N_n^{2\text{B}} \frac{\Gamma_2}{\Gamma_1} - \left(N_p^{1\text{Bp}} + N_p^{2\text{B}} \frac{\Gamma_2}{\Gamma_1} \right) \frac{N_n}{N_p}}{\left(N_p^{1\text{Bn}} + N_p^{2\text{B}} \frac{\Gamma_2}{\Gamma_1} \right) \frac{N_n}{N_p} - N_n^{1\text{Bn}} - N_n^{2\text{B}} \frac{\Gamma_2}{\Gamma_1}}, \quad (3.5)$$

where:

$$N_N^{2B} = \frac{N_N^{2Bnn}\Gamma_{nn} + N_N^{2Bnp}\Gamma_{np} + N_N^{2Bpp}\Gamma_{pp}}{\Gamma_{nn} + \Gamma_{np} + \Gamma_{pp}}. \quad (3.6)$$

Using our predictions of Tables I and II together with the datum of KEK–E508 [6], $N_n/N_p = 2.00 \pm 0.17$, we obtain:

$$\frac{\Gamma_n}{\Gamma_p} = 0.95 \pm 0.21. \quad (3.7)$$

Neglecting the $2N$ –stimulated channel the result is:

$$\left(\frac{\Gamma_n}{\Gamma_p}\right)^{1N} = 0.88 \pm 0.16, \quad (3.8)$$

while enhancing arbitrarily the $2N$ –induced rates by a factor of two we obtain:

$$\left(\frac{\Gamma_n}{\Gamma_p}\right)^{\Gamma_2 \rightarrow 2\Gamma_2} = 1.02 \pm 0.27. \quad (3.9)$$

The sensitivity of the ratio Γ_n/Γ_p to the values of the $2N$ –induced decay widths turns out to be moderate, especially if the error bars originated by the datum adopted for N_n/N_p are taken into account. This is due not only to the negligible role of the $2N$ –stimulated processes in Eq. (3.5) ($N_{n(p)}^{1Bp}$ and $N_{n(p)}^{1Bn}$ are larger than $N_{n(p)}^{2B}\Gamma_2/\Gamma_1$ since a quite high energy threshold is employed), but also to the particular value of N_n/N_p used in the analysis, which causes a certain cancellation among the $2N$ –stimulated contributions in both the numerator and denominator of Eq. (3.5): $N_n^{2B} \simeq N_p^{2B}N_n/N_p$. Such a cancellation would be complete, thus leading to the extraction of the same central value of Γ_n/Γ_p for any value of Γ_2 , if a ratio $N_n/N_p = N_n^{2B}/N_p^{2B} = 1.65$ were used in the analysis.

These occurrences can be understood from Figure 7, which shows the relation between the observable ratio N_n/N_p and Γ_n/Γ_p for different choices of Γ_2/Γ_1 . The dotted line corresponds to the case in which $2N$ –induced decays and FSI are neglected. Once FSI are incorporated, quite different dependencies are obtained. The dot–dashed line refers to the calculation in which Γ_2 is set to 0, the continuous line to the Γ_2/Γ_1 ratio predicted by the present LDA model and the dashed line to the case in which the size of Γ_2 is arbitrarily doubled.

Note in particular that the previously extracted Γ_n/Γ_p values are different from the value 0.5 given in Ref. [6] and expected on the basis of the relation $\Gamma_n/\Gamma_p = (N_n/N_p - 1)/2$, which holds if $2N$ –induced decays and FSI effects are ignored, i.e., if $N_n^{1Bn} = 2$, $N_n^{1Bp} = N_p^{1Bp} = 1$, $N_p^{1Bn} = N_{n(p)}^{2Bnn} = N_{n(p)}^{2Bnp} = N_{n(p)}^{2Bpp} = 0$ in Eqs. (3.5) and (3.6) (see the point where the experimental datum intersects the dotted line in Fig. 7). Contrary to the claim of Ref. [6] and according to our results, FSI turn out to be rather important even when one discusses the number ratio N_n/N_p (for which part of the FSI effect is certainly canceled out) and uses high kinetic thresholds such as 60 MeV. On the contrary, it is well manifest from Fig. 7

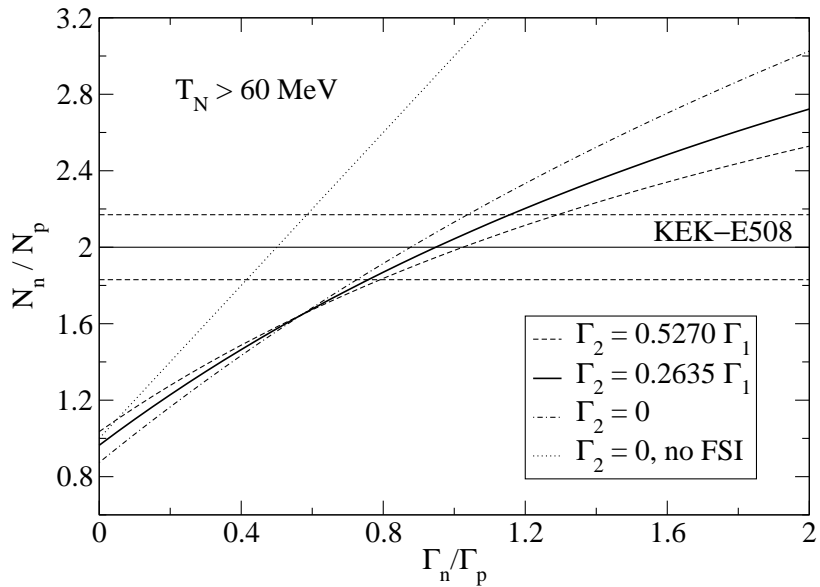


FIG. 7. Dependence of the observable ratio N_n/N_p on Γ_n/Γ_p and Γ_2/Γ_1 for a nucleon energy threshold of 60 MeV. The horizontal lines show KEK-E508 data [6]. See text for further details.

that the $2N$ -induced decay mechanism plays a relatively small role in the whole range of reasonable Γ_n/Γ_p values.

We also note that a naif estimation of FSI, such as that performed by Kim et al. [5] (which also neglect the $2N$ -induced mechanism) taking a ratio $g/f = 0.11$, where f is the loss factor of each nucleon type and g the influx factor of one nucleon type converted from the other type, gives $\Gamma_n/\Gamma_p = 0.71 \pm 0.14$ (see Eq.(4) of Ref. [5]). Although, due to error bars, this result is quite compatible with the one obtained here with a more realistic treatment of FSI and disregarding $2N$ -stimulated decays, $\Gamma_n/\Gamma_p = 0.88 \pm 0.16$, clearly, the difference between the two central values demonstrates the following fact: that a detailed account of FSI do not support the method used in Ref. [5] to determine Γ_n/Γ_p .

We finalize this subsection by remarking that large ratios such as those of Eqs.(3.7)–(3.9) turn out to strongly overestimate the value (0.285) predicted by the weak decay model employed in the present paper. Actually, no calculation performed up to date reproduces these determinations, which are more in agreement with the previous single-proton data of Refs. [4,29,30], as summarized in Table I. Only the presence of an isoscalar, spin-independent central operator in the weak transition potential can reproduce larger Γ_n/Γ_p values, as can be inferred from the effective treatment of Ref. [26].

C. Double coincidence nucleon spectra

Now we discuss the NN coincidence spectra obtained from our model for the decay of $^{12}\Lambda\text{C}$. Figs. 8 and 9 show, respectively, the distribution of nn and np pairs, as a function

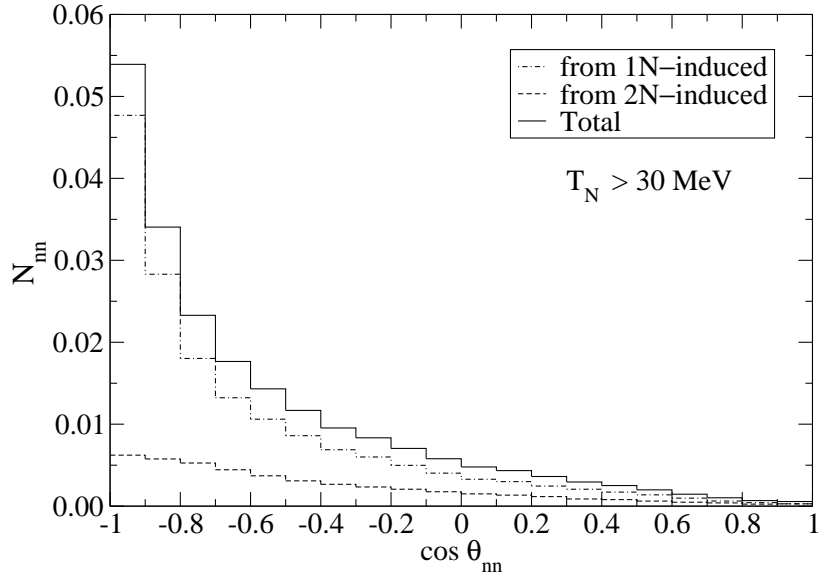


FIG. 8. Opening angle distribution of nn pairs normalized per non-mesonic weak decay.

of the cosine of the opening angle, where FSI effects have been incorporated and a kinetic energy cut of 30 MeV has been applied. We observe that the distribution of pairs from the $1N$ -induced processes (dash-dotted line) is more back-to-back dominated than that coming from the $2N$ -induced processes (dashed line). In any case, the $1N$ -induced channel still provides the larger contribution of pairs in the whole range of opening angles.

For $\cos \theta_{NN} \lesssim -0.4$ the results of Figs. 8 and 9 reasonably reproduces the ones of the previous finite nucleus calculation reported in Fig. 5 of Ref. [14] and Fig. 9 of Ref. [15]. On the contrary, for $\cos \theta_{NN} \gtrsim -0.4$ a discrepancy is evident, the finite nucleus distributions being nearly flat in this region and the nuclear matter ones going monotonously to almost vanishing values with $\cos \theta_{NN}$. This is ascribable to the different phase space treatment in the two approaches. Indeed, the fact that the nuclear matter calculation exhibits a more pronounced Fermi motion effect (see Fig. 3) gives rise to a smaller number of outgoing nucleons with respect to the finite nucleus case (see Fig. 4). This, in turn, is responsible for the fact that the final nucleons of the finite nucleus calculation are more distorted by FSI than the nucleons in the nuclear matter approach. As a final result, the NN opening angle distributions are more back-to-back correlated in the nuclear matter calculation.

Our distributions of Figs. 8 and 9 can also be compared with those obtained by KEK-E508 and shown in Figure 3 of the recent preprint by Kim et al. [10]. Due to the limited statistics of data, we concentrate on the angular region with $\cos \theta_{NN} < -0.7$. In this region, experiment predicts $N_{nn} = 0.083 \pm 0.014$ and $N_{np} = 0.138 \pm 0.014$, whereas our corresponding results are $N_{nn} = 0.111$ and $N_{np} = 0.300$, these numbers being normalized

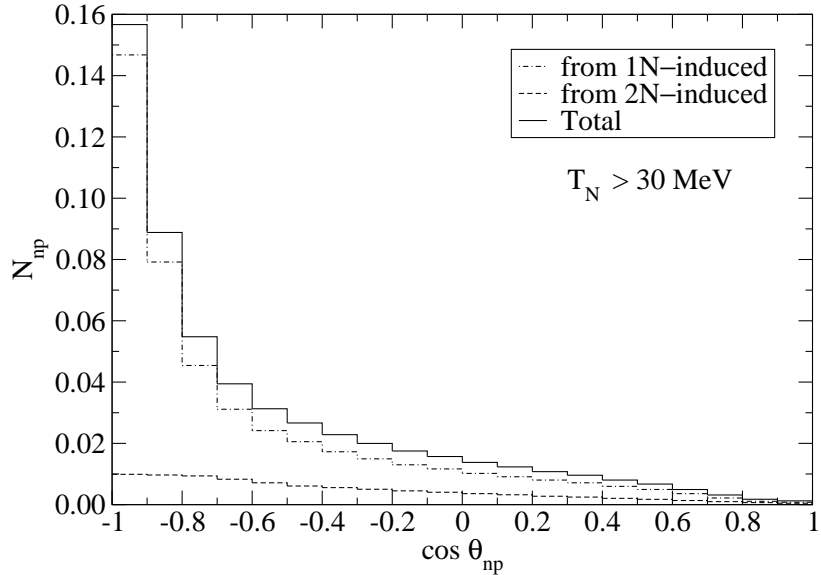


FIG. 9. Opening angle distribution of np pairs normalized per non-mesonic weak decay.

per non-mesonic weak decay. While there is decent agreement in the case of N_{nn} , for N_{np} we overestimate the datum by a factor of about 2. The origin of such a discrepancy is likely the same as the one responsible for the disagreement on the single-proton spectra of Fig. 4. Another indication supporting this hypothesis comes from comparing our result for the number of proton-proton pairs for $T_N^{\text{th}} = 30$ MeV and $\cos \theta_{NN} < -0.7$, $N_{pp} = 0.050$, with the experimental value $N_{pp} = 0.005 \pm 0.002$. One cannot exclude the possibility that the experiment systematically underestimated the number of protons emitted in $^{12}\Lambda$ decay, thus leading to an underestimation of N_p , N_{np} and N_{pp} spectra. On the contrary, for the observables involving only neutron detection, N_n and N_{nn} , theory and experiment are in reasonable accordance.

The nn and np pair distribution as functions of the total kinetic energy of the pair is shown in Figs. 10 and 11, respectively, where the energy of each nucleon is larger than a threshold kinetic energy of 30 MeV. The upper panels show the distributions obtained without any cut in the opening angle, while in the bottom panels only the back-to-back events are kept by applying the restriction $\cos \theta_{NN} < -0.7$. We observe that the $2N$ -induced events (dashed lines) in the upper panels scarcely contribute at the position of the primary peak of the $1N$ -induced contribution (dot-dashed lines). Instead, they enhance the total distribution at a pair energy of around 100 MeV and generate a secondary peak there, which might become even larger (see the case of the nn pairs) than the primary one at the Q -value of about 155 MeV. When the angular cut is applied, many of the events in the low energy region are removed and the so-called back-to-back peak at 155 MeV stands

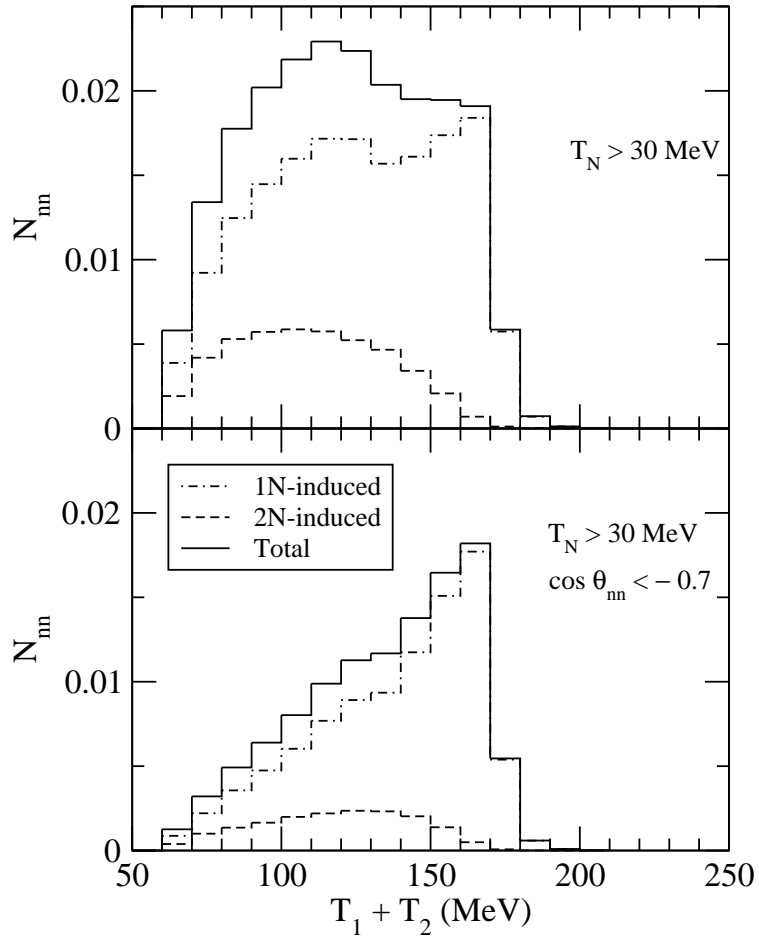


FIG. 10. Distribution of the total kinetic energy of nn pairs normalized per non-mesonic weak decay. The energy threshold is 30 MeV for each nucleon in the pair. In the upper panel there is no angular restriction, while the condition $\cos \theta_{nn} < -0.7$ has been imposed in the results of the lower panel.

out more clearly. However, there is still an important fraction of the events (about 2/3 of nn pairs and about 1/2 of np pairs) that lie outside this peak. This is in quantitative agreement with the finite nucleus results of our previous works (see Fig. 3 of Ref. [14] and Fig. 10 of Ref. [15]), the only qualitative difference being the width of the back-to-back peak, which appears more smeared out in the present work due to a more marked effect of Fermi motion. In particular, note how the distributions from $1N$ -induced decays of Figs. 10 and 11 extend above the Q -value of the non-mesonic decay.

D. 2N-induced strength

In this subsection we compare the results of our microscopic model for the $2N$ -induced channel with those of the phenomenological model of Ref. [33]. We also analyze here the

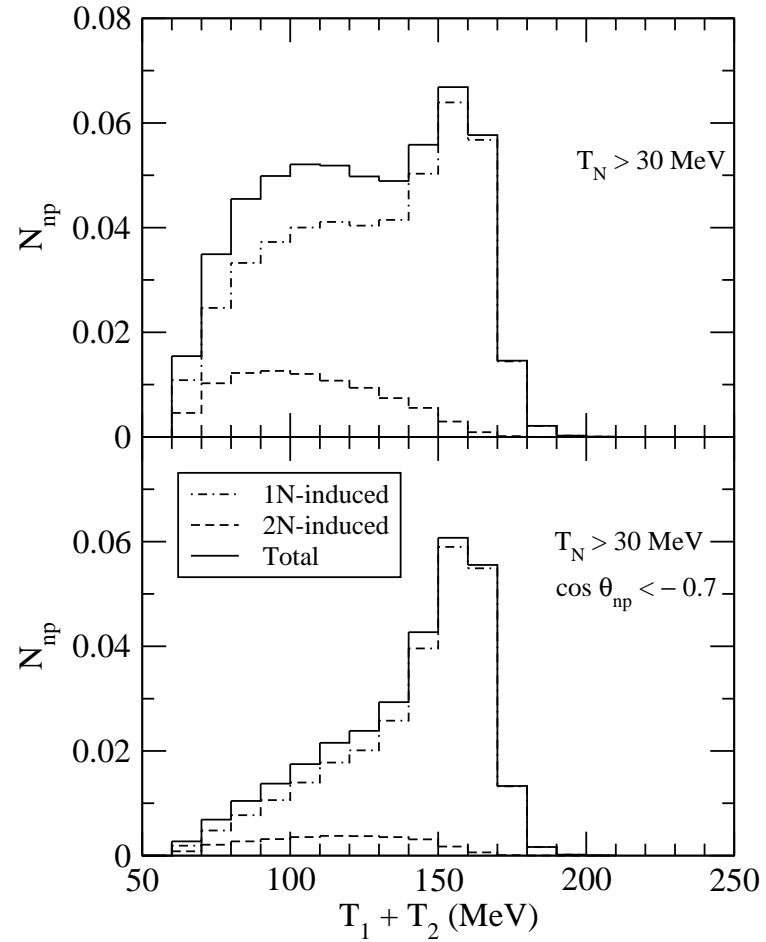


FIG. 11. Distribution of the total kinetic energy of np pairs normalized per non-mesonic weak decay. The energy threshold is 30 MeV for each nucleon in the pair. In the upper panel there is no angular restriction, while the condition $\cos \theta_{np} < -0.7$ has been imposed in the results of the lower panel.

distribution of NN pairs from the various sources of $2N$ –induced strength.

We start by commenting on the claim stated in Ref. [6] about the existence of two different types of $2N$ –induced decay. One would be a “three–body reaction”, in which the available energy is equally shared among the three final nucleons, while the other one should be due to the absorption of the pion emitted at the weak vertex by a correlated two–nucleon pair. According to Ref. [6], in our previous calculations [14,15], where the $2N$ –induced strength was taken from the model of Ref. [33], we only included the latter. Here we want to clarify that there is in fact only one type of $2N$ –induced non–mesonic decay and that the particular kinematical properties of the emitted particles, prior to FSI, are dictated by the dynamics of the $2N$ –induced decay mechanism. In the one–pion–exchange model of Ref. [33] the absorption by a correlated nucleon pair of the virtual pion emitted at the Λ vertex is driven by a phenomenological two particle–two hole polarization propagator $\Pi_{2p2h}(q^0, \mathbf{q})$. In the limit $(q^0, \mathbf{q}) \rightarrow (m_\pi, 0)$ this propagator describes the absorption of real pions in nuclear matter but we note that it was conveniently extended, via a phase space correction, to account for all possible (q^0, \mathbf{q}) values of the exchanged virtual pion. Nevertheless, the pion at the Λ vertex turns out to be preferentially close to its mass shell and, consequently, the nucleon emitted at the same vertex has very little kinetic energy left, whereas the other two nucleons of the $2N$ –induced channel are quite energetic and come out in a back–to–back geometry. This is illustrated in Fig. 12, that shows the distribution of momentum values for each of the three nucleons emitted by the $2N$ –induced mechanism, prior to FSI effects. The left panel shows the distribution obtained from the phenomenological model. It is clearly seen that the nucleon emitted at the Λ vertex, whose momentum is denoted by p_1 , is very slow while the other two are equally fast, having momenta on average of about 400 MeV/c. In contrast, in the microscopic one–meson–exchange model of Ref. [20] used in the present work, the nucleon emitted at the bubble that absorbs the exchanged meson (see Fig. 2) can reach high p_2 momentum values by combining the momentum q of the virtual meson plus the momentum p'_2 of the correlated nucleon that can be large due to the short range nature of the NN interaction. The momentum p_1 , carried by the nucleon emitted at the Λ vertex, and the momentum p_3 , corresponding to the nucleon from the spectator bubble, will acquire values characteristic of the range of the interaction they come out from, which is, respectively, the weak and strong one–meson–exchange models used in Ref. [20]. As we observe in the right panel of Fig. 12, the distributions of p_1 and p_3 momentum values turn out to be quite similar, peaking around 300 MeV/c, while that for p_2 peaks at higher momentum values close to 500 MeV/c.

We now compare the phenomenological and microscopic models after the three primary nucleons emitted in the weak decay process are allowed to undergo collisions with the other nucleons as they move out of the nucleus. We restrict here to the np –induced decay mode, which is the most important one in the microscopic approach and the only one considered by the phenomenological model. The distribution of np pairs, normalized per its corresponding np –induced transition rate, is shown in Fig. 13 as a function of the opening angle, where

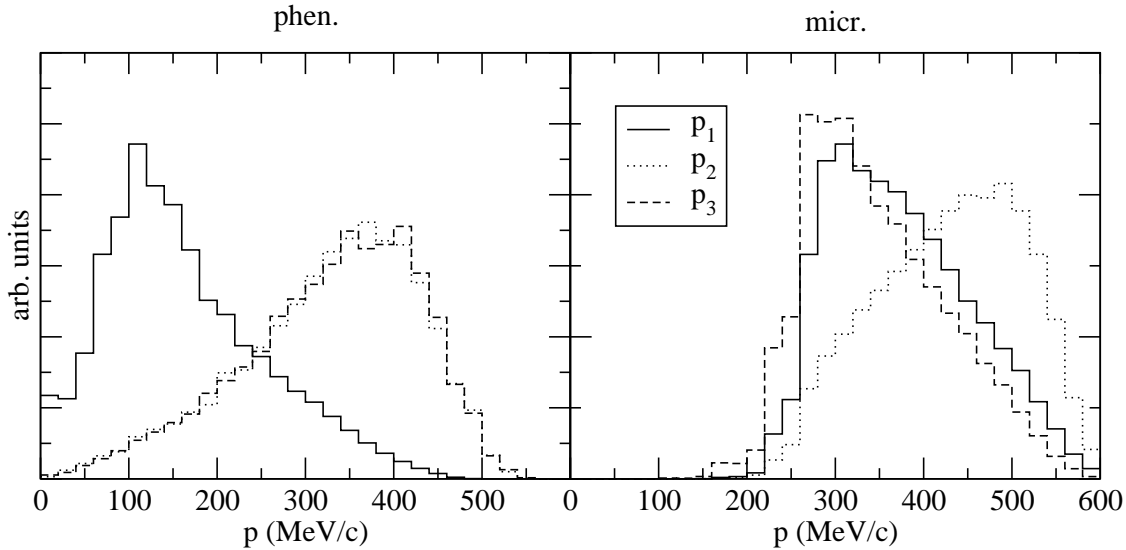


FIG. 12. Momentum distribution of each of the three primary nucleons emitted in $2N$ –induced processes.

the threshold kinetic energy is 30 MeV for each nucleon of the pair. The dotted (solid) line shows the results without (with) FSI effects. It is clear that, at variance to the microscopical approach, the phenomenological model produces a distinct back–to–back distribution which stands quite clearly even when FSI effects are included. The distribution of pairs as a function of the total kinetic energy and for a threshold $T_N^{\text{th}} = 30$ MeV is displayed in Fig. 14. We observe that the amount of N_{np} pairs per np –induced decay event in the absence of FSI (area under the dotted curves) is smaller in the phenomenological model, since the slow nucleon is always eliminated by the kinetic energy cut of 30 MeV. This situation is compensated when the opening angle cut is also applied (dashed lines), since it removes more events in the microscopic distribution, which is not so back–to–back dominated. The conclusion is that, even if the kinematics of the primary nucleons look quite different, at the end, once the effect of FSI is considered and the energy and angular cuts are applied, both models produce similar neutron–proton angular and energy spectra per np –induced decay event.

We now discuss the distribution of the various contributions (nn –, np – and pp –induced) to the $2N$ –induced non–mesonic decay in the microscopic model. The opening angle distribution of nn and np pairs, again for $T_N^{\text{th}} = 30$ MeV, is shown, respectively, on the left and right panels of Fig. 15. The angular distribution of both nn and np pairs decreases smoothly with increasing $\cos \theta_{NN}$. We observe that the most important contribution is that of the np –induced decay, as we expected from the values of the decay rates shown in Table I. We note also that there is a small amount of nn pairs from the pp –induced process and np pairs from the nn –induced one which would be zero in the absence of FSI.

The total pair energy distribution from the $2N$ –induced channels is shown in Fig. 16,

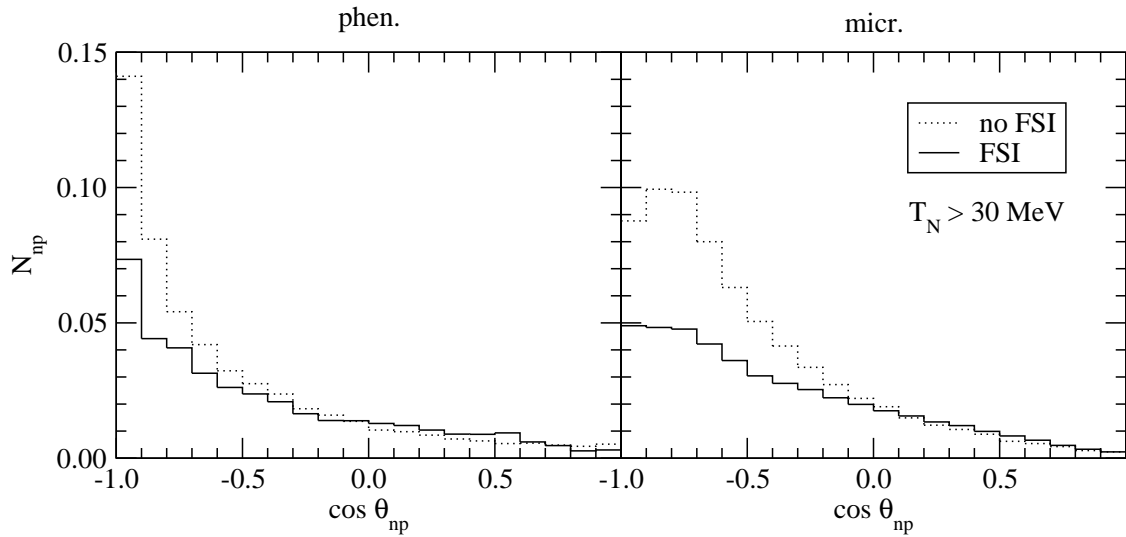


FIG. 13. Opening angle distribution of np pairs from the np -induced channel, normalized per np -induced decay.

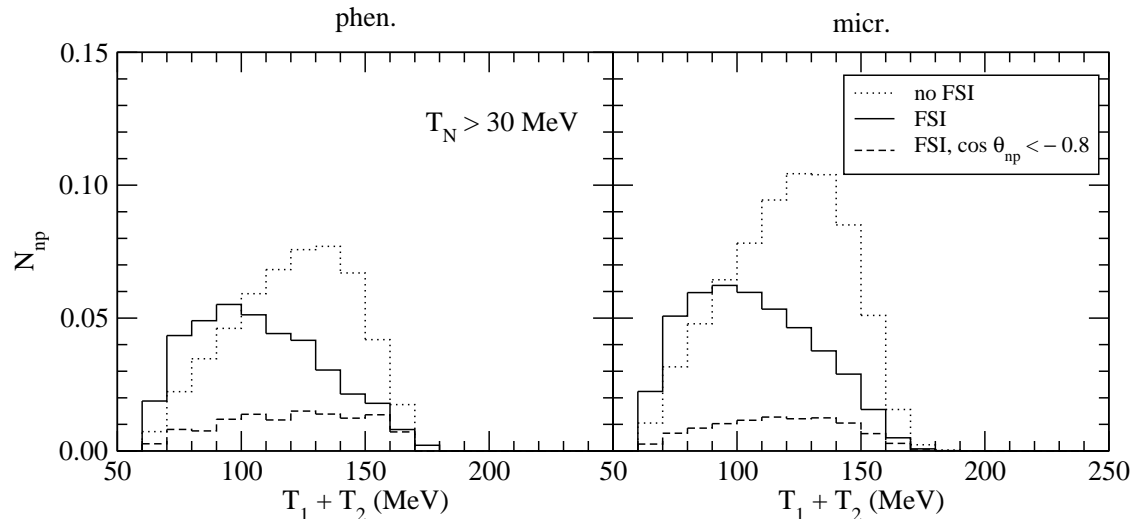


FIG. 14. Total kinetic energy distribution of np pairs from the np -induced channel, normalized per np -induced decay.

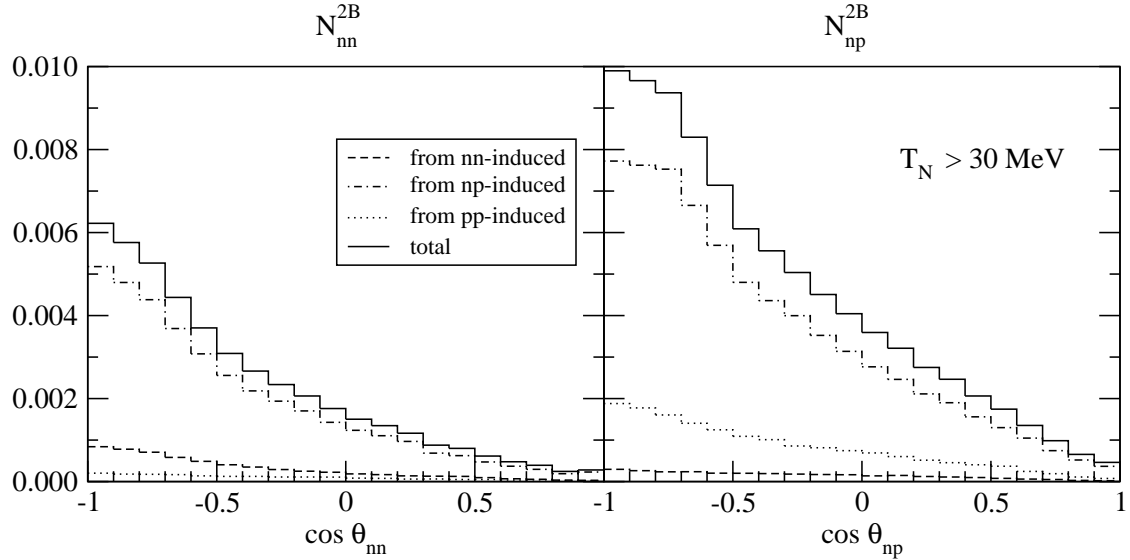


FIG. 15. Various $2N$ -induced contributions ($2N = nn, np, pp$) to the opening angle distribution of nn (left) and np pairs (right). All results are normalized per total non-mesonic weak decay.

where an angular cut of $\cos \theta_{NN} < -0.8$ has been applied in addition to $T_N^{\text{th}} = 30$ MeV. The dominance of the np -induced decay is obvious from figures 15 and 16, although after applying the usual kinetic and angular cut-offs the strength of some channels, as e.g. the pp -channel contributing to the number of np pairs, can represent up to 20% of the total.

E. Ratio N_{nn}/N_{np}

We now discuss a comparison of our predictions for the ratio between the number of nn and np pairs for ^{12}C with experimental determinations by KEK-E508 [7–10]. As in previous papers [14,15], we introduce the numbers of NN pairs ($NN = nn, np$ or pp) coming from one-nucleon induced ($N_{NN}^{1\text{Bn}}$ and $N_{NN}^{1\text{Bp}}$) and two-nucleon induced ($N_{NN}^{2\text{Bnn}}$, $N_{NN}^{2\text{Bnp}}$ and $N_{NN}^{2\text{Bpp}}$) processes, each one of them being normalized per the rate of the corresponding process. These weak decay model independent quantities are given in Table III for nucleon kinetic energies $T_N \geq 30$ MeV and two angular regions. The total number of NN pairs emitted per non-mesonic weak decay event can be built from:

$$\begin{aligned} N_{NN} &= \frac{N_{NN}^{1\text{Bn}}\Gamma_n + N_{NN}^{1\text{Bp}}\Gamma_p + N_{NN}^{2\text{Bnn}}\Gamma_{nn} + N_{NN}^{2\text{Bnp}}\Gamma_{np} + N_{NN}^{2\text{Bpp}}\Gamma_{pp}}{\Gamma_n + \Gamma_p + \Gamma_{nn} + \Gamma_{np} + \Gamma_{pp}} \\ &= \frac{N_{NN}^{1\text{Bn}}\Gamma_n + N_{NN}^{1\text{Bp}}\Gamma_p + N_{NN}^{2\text{B}}\Gamma_2}{\Gamma_n + \Gamma_p + \Gamma_2}, \end{aligned} \quad (3.10)$$

where:

$$N_{NN}^{2\text{B}} = \frac{N_{NN}^{2\text{Bnn}}\Gamma_{nn} + N_{NN}^{2\text{Bnp}}\Gamma_{np} + N_{NN}^{2\text{Bpp}}\Gamma_{pp}}{\Gamma_{nn} + \Gamma_{np} + \Gamma_{pp}} \quad (3.11)$$

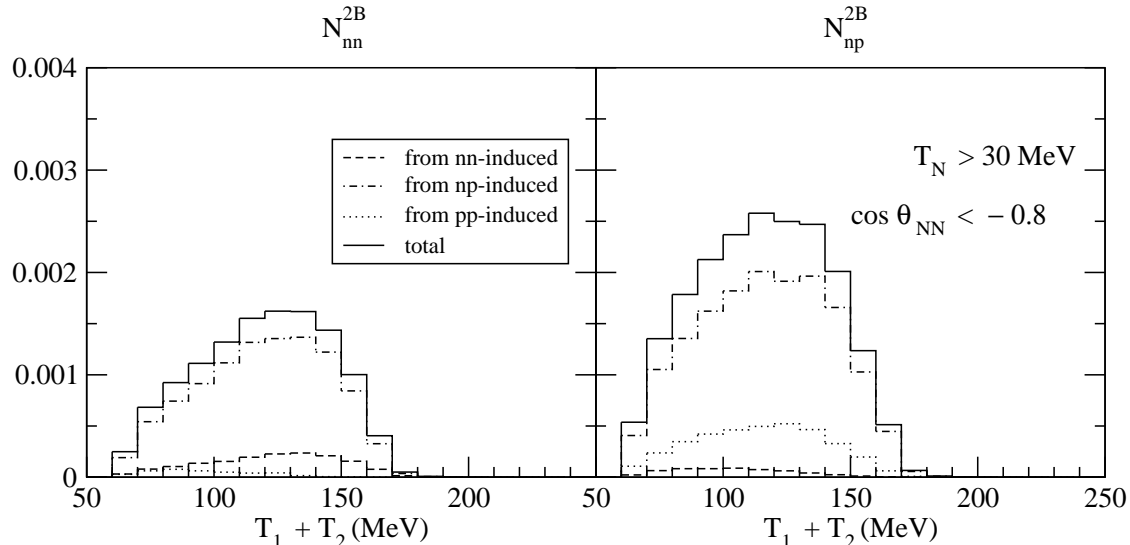


FIG. 16. Various $2N$ –induced contributions ($2N = nn, np, pp$) to the pair kinetic energy distribution of nn (left) and np pairs (right). All results are normalized per total non–mesonic weak decay.

evidently depends on the weak model employed.

Before proceeding with the discussion on the ratio N_{nn}/N_{np} , we want to compare the results of Table III with the ones obtained within the finite nucleus framework of Refs. [14,15] and reported in Table IV. A very good agreement is noticeable for the $1N$ –induced contributions. That is expected and depends on the fact that 1) the considered numbers are independent of the weak decay model one uses and 2) the FSI effects are modeled with the same intranuclear cascade code in both evaluations. Possible differences have to be ascribed to the different frameworks (finite nucleus vs nuclear matter) used for describing hypernuclear structure effects. The disagreement existing for some $2N$ –induced contributions, whose significance are anyhow relatively low for the total numbers N_{NN} due to the smallness of the corresponding decay rates, is due to the different decay channels and (especially) phase space factors involved in the two determinations (for a comparison of the phase spaces, we refer to the discussion of Fig. 12).

We now come back to the N_{nn}/N_{np} ratio. From Eq. (3.10) and our results of Tables I and III we obtain:

$$\frac{N_{nn}}{N_{np}} = 0.36 \quad (3.12)$$

for the case with $\cos \theta_{NN} \leq 0.8$. This is in good agreement with the KEK–E508 datum 0.40 ± 0.10 [7]. The comparison of the result (3.12) with those obtained with the calculations of Ref. [15] (from Tables I and IV), namely $N_{nn}/N_{np} = 0.43$ and 0.47 , using the OMEa and OMEf models, respectively, show the differences in the partial decay rates and phase spaces predicted by the different models. If the $2N$ –stimulated decay mode is neglected, the present

TABLE III. Predictions for the weak interaction model independent quantities N_{NN}^{1Bn} , N_{NN}^{1Bp} , N_{NN}^{2Bnn} , N_{NN}^{2Bnp} , N_{NN}^{2Bpp} and for N_{NN}^{2B} of Eqs. (3.10) and (3.11) for $^{12}\Lambda$ C, integrated over all opening angles and for nucleon energies $T_N \geq 30$ MeV. The numbers in parentheses correspond to the angular region with $\cos \theta_{NN} \leq -0.8$.

N_{nn}^{1Bn}	N_{nn}^{1Bp}	N_{nn}^{2Bnn}	N_{nn}^{2Bnp}	N_{nn}^{2Bpp}	N_{nn}^{2B}
0.55 (0.31)	0.11 (0.03)	0.53 (0.15)	0.24 (0.06)	0.05 (0.01)	0.22 (0.06)
N_{np}^{1Bn}	N_{np}^{1Bp}	N_{np}^{2Bnn}	N_{np}^{2Bnp}	N_{np}^{2Bpp}	N_{np}^{2B}
0.34 (0.09)	0.64 (0.34)	0.27 (0.05)	0.45 (0.10)	0.40 (0.09)	0.43 (0.09)
N_{pp}^{1Bn}	N_{pp}^{1Bp}	N_{pp}^{2Bnn}	N_{pp}^{2Bnp}	N_{pp}^{2Bpp}	N_{pp}^{2B}
0.04 (0.01)	0.15 (0.05)	0.02 (0.004)	0.08 (0.02)	0.30 (0.08)	0.12 (0.03)

TABLE IV. Predictions of the finite nucleus calculation of Ref. [15] for the weak interaction model independent quantities N_{NN}^{1Bn} , N_{NN}^{1Bp} and for N_{NN}^{2B} (integrated over all angles and for nucleon energies $T_N \geq 30$ MeV) for $^{12}\Lambda$ C. The numbers in parentheses correspond to the angular region with $\cos \theta_{NN} \leq -0.8$.

N_{nn}^{1Bn}	N_{nn}^{1Bp}	N_{nn}^{2B}
0.57 (0.31)	0.11 (0.03)	0.30 (0.12)
N_{np}^{1Bn}	N_{np}^{1Bp}	N_{np}^{2B}
0.34 (0.09)	0.68 (0.32)	0.39 (0.10)
N_{pp}^{1Bn}	N_{pp}^{1Bp}	N_{pp}^{2B}
0.04 (0.01)	0.17 (0.05)	0.05 (0.01)

calculation predicts:

$$\left(\frac{N_{nn}}{N_{np}} \right)^{1N} = 0.34, \quad (3.13)$$

thus emphasizing a relatively small effect of the $2N$ -induced channels on correlation observables appropriately chosen. The above result (3.13) should be compared with the naïf estimation $N_{nn}/N_{np} = \Gamma_n/\Gamma_p = 0.285$ obtained by neglecting both FSI and the $2N$ -induced decay channel: contrary to what occurs to single-nucleon spectra, i.e., to N_n/N_p , the effect of FSI in the present case of coincidence observables turns out to be not too marked. The reliability of the above naïf equality improves by using higher thresholds T_N^{th} and more restrictive back-to-back constraints. We can therefore conclude that, for the cases of experimental interest such as those considered here and in Section III B, the equation $N_{nn}/N_{np} = \Gamma_n/\Gamma_p$ turns out to have a wider range of approximate validity than the assumption $N_n/N_p = (2\Gamma_n + \Gamma_p)/\Gamma_p$ sometimes used in experimental analyses, whose utilization to estimate Γ_n/Γ_p must be avoided.

We now consider a weak decay model independent analysis of the N_{nn}/N_{np} data of Table V to determine Γ_n/Γ_p . These data have been obtained by KEK for ${}^5\Lambda\text{He}$ [9] and ${}^{12}\Lambda\text{C}$ [7,10] with a threshold $T_N^{\text{th}} = 30$ MeV and various angular restrictions. The ratio Γ_n/Γ_p is determined by using theoretical values for Γ_{nn}/Γ_1 , Γ_{np}/Γ_1 and Γ_{pp}/Γ_1 and data for N_{nn}/N_{np} from:

$$\frac{\Gamma_n}{\Gamma_p} = \frac{N_{nn}^{1\text{Bp}} + N_{nn}^{2\text{B}} \frac{\Gamma_2}{\Gamma_1} - \left(N_{np}^{1\text{Bp}} + N_{np}^{2\text{B}} \frac{\Gamma_2}{\Gamma_1} \right) \frac{N_{nn}}{N_{np}}}{\left(N_{np}^{1\text{Bn}} + N_{np}^{2\text{B}} \frac{\Gamma_2}{\Gamma_1} \right) \frac{N_{nn}}{N_{np}} - N_{nn}^{1\text{Bn}} - N_{nn}^{2\text{B}} \frac{\Gamma_2}{\Gamma_1}}, \quad (3.14)$$

where $N_{NN}^{2\text{B}}$ is given by Eq. (3.11). From our predictions of Tables I and III and the ${}^{12}\Lambda\text{C}$ datum of KEK-E508 derived with the restrictions $T_N \geq 30$ MeV and $\cos \theta_{NN} \leq -0.8$ we obtain:

$$\frac{\Gamma_n}{\Gamma_p} = 0.34 \pm 0.15. \quad (3.15)$$

Besides, neglecting the $2N$ -stimulated channel:

$$\left(\frac{\Gamma_n}{\Gamma_p} \right)^{1N} = 0.37 \pm 0.14, \quad (3.16)$$

while enhancing arbitrarily the $2N$ -induced rates by a factor of two:

$$\left(\frac{\Gamma_n}{\Gamma_p} \right)^{\Gamma_2 \rightarrow 2\Gamma_2} = 0.32 \pm 0.16. \quad (3.17)$$

The ratio (3.15) [(3.16)] must be compared with $\Gamma_n/\Gamma_p = 0.27 \pm 0.14$ [$\Gamma_n/\Gamma_p = 0.36 \pm 0.14$] obtained from the results of Ref. [15] (listed in Table IV) together with a value of $\Gamma_2/\Gamma_1 =$

TABLE V. $^5_{\Lambda}\text{He}$ [9] and $^{12}_{\Lambda}\text{C}$ [7,10] KEK data for the ratio N_{nn}/N_{np} corresponding to a nucleon threshold $T_N^{\text{th}} = 30$ MeV and different opening angle regions. The corresponding determinations of Γ_n/Γ_p obtained in the present work and from the results of Ref. [15] are also reported.

Angular range	$^5_{\Lambda}\text{He}$		$^{12}_{\Lambda}\text{C}$	
	N_{nn}/N_{np}	Γ_n/Γ_p [15]	N_{nn}/N_{np}	Γ_n/Γ_p [this work]
$\cos \theta_{NN} \leq -0.9$			0.45 ± 0.12	0.43 ± 0.17
$\cos \theta_{NN} \leq -0.8$	0.45 ± 0.11	0.27 ± 0.11	0.40 ± 0.10	0.34 ± 0.15
$\cos \theta_{NN} \leq -0.7$			0.60 ± 0.12	0.66 ± 0.24

0.25 used there. While the ratios are very similar when $\Gamma_2 = 0$, a certain difference is obtained for those including $2N$ –stimulated decay effects. This is quite obvious and signals the different models used in the two works for the $2N$ –induced channels.

In Figure 17 we show the relation between N_{nn}/N_{np} and Γ_n/Γ_p for different choices of Γ_2/Γ_1 and for $T_N^{\text{th}} = 30$ MeV and $\cos \theta_{NN} \leq -0.8$. The dotted line corresponds to the case in which $2N$ –induced decays and FSI are neglected. Different behaviours are obtained once FSI are incorporated. The dot–dashed line refers to the calculation in which Γ_2 is set to 0, the continuous line to the Γ_2/Γ_1 ratio predicted by the present LDA model and the dashed line to the case in which the size of Γ_2 is arbitrarily doubled. The comparison of Fig. 17 with Fig. 7 clearly illustrates the fact that FSI affect much more the extraction of Γ_n/Γ_p from N_n/N_p than from N_{nn}/N_{np} .

Table V summarizes the values of Γ_n/Γ_p derived in our analysis of KEK data for N_{nn}/N_{np} in $^{12}_{\Lambda}\text{C}$. Also reported is the result for $^5_{\Lambda}\text{He}$ of the finite nucleus calculation of Ref. [15]. In all cases the values reported for Γ_n/Γ_p have been obtained by including the $2N$ –stimulated contributions as predicted by the two different approaches. As a signal of the limited statistics of the data employed, the central value for Γ_n/Γ_p in $^{12}_{\Lambda}\text{C}$ shows a certain undesired dependence on the opening angle region. Nevertheless, the error bars are so big that values in the interval 0.4–0.5 are common to all determinations. The final result can thus be given by the weighted average of the three partial results:

$$\left(\frac{\Gamma_n}{\Gamma_p} \right)^{\text{best}} = 0.43 \pm 0.10. \quad (3.18)$$

When $2N$ –induced decay channels are neglected, a similar analysis of data supplies a very close “best” value:

$$\left(\frac{\Gamma_n}{\Gamma_p} \right)^{1N \text{ best}} = 0.46 \pm 0.09. \quad (3.19)$$

We want to note that for the case with $\cos \theta_{NN} \leq -0.7$, Kim et al. [10] have recently extracted a ratio $\Gamma_n/\Gamma_p = 0.51 \pm 0.13 \pm 0.04$ by employing the number of detected proton–proton pairs in addition to the measurement of N_{nn} and N_{np} . A schematic method for

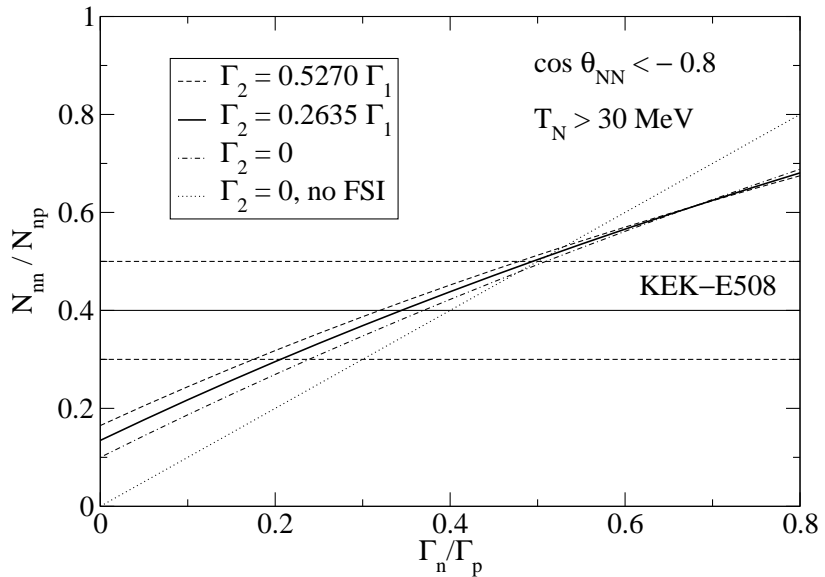


FIG. 17. Dependence of the observable ratio N_n/N_p on Γ_n/Γ_p and Γ_2/Γ_1 for a nucleon energy threshold of 30 MeV and $\cos \theta_{NN} \leq -0.8$. The horizontal lines show KEK-E508 data [7]. See text for further details.

accounting for FSI effects, similar to the one employed in Ref. [5] for single-nucleon observables, was adopted for this purpose. In addition, $2N$ -stimulated decay channels were neglected. The discrepancy between this KEK determination and our detailed prediction of Table V for $\cos \theta < -0.7$ (compare especially the central values) demonstrate that analyses of data such as those of Refs. [5,10] show certain limitations.

IV. CONCLUSIONS

We have presented a study of single- and double-coincidence nucleon spectra for the non-mesonic weak decay of Λ -hypernuclei. One-meson-exchange models have been used to describe one- and two-nucleon induced decay processes, $\Lambda N \rightarrow nN$ and $\Lambda NN \rightarrow nNN$, in a nuclear matter framework which has been adapted for finite nuclei predictions via the local density approximation. Besides, an intranuclear cascade code based on Monte Carlo techniques has simulated the final state interactions of the outgoing nucleons with the residual nucleus.

Unlike previous papers, here we have adopted a microscopic approach for describing the two-nucleon induced decay, which included the channels $\Lambda nn \rightarrow nnn$ and $\Lambda pp \rightarrow npp$ in addition to the mode $\Lambda np \rightarrow nnp$ already considered in previous phenomenological studies. The use of a different theoretical approach for calculation meets our main purpose of making the extraction of the ratio Γ_n/Γ_p from data less model dependent.

The results have been compared with previous finite nucleus analyses [14,15], with special

consideration for the two–nucleon induced decay mechanism, and with a considerable amount of recent data by KEK [5–10]. Apart from some difference ascribable to the phase space dependence and to the different weak decay models adopted for the two–nucleon induced decay channels, the present predictions for the observable ratios N_n/N_p and N_{nn}/N_{np} confirm the finite nucleus results.

The single–neutron spectra for $^{12}\Lambda\text{C}$ and $^{89}\Lambda\text{Y}$ measured by KEK–E369 and KEK–E508 have been reproduced with reasonable accuracy. On the contrary, the KEK–E508 single–proton spectrum for $^{12}\Lambda\text{C}$ is in strong disagreement with our prediction. The theoretical distribution would reproduce these data only by enforcing artificially large values for Γ_n/Γ_p , which, in turn, would lead to a serious overestimation of the mentioned single–neutron spectra. As a consequence of that, through the weak interaction model independent analysis of N_n/N_p data for $^{12}\Lambda\text{C}$ we determined $\Gamma_n/\Gamma_p = 0.95 \pm 0.21$, a value that largely overestimates pure theoretical predictions ranging between 0.3 and 0.5.

The contribution of the two–nucleon induced decay channels in these analyses turn out to be of moderate size when high nucleon kinetic energy cuts such as 60 MeV are imposed. On the contrary, FSI effects reveal to be of great importance when determining Γ_n/Γ_p from single–nucleon data. A demonstration of that is the inapplicability of the relation $\Gamma_n/\Gamma_p = (N_n/N_p - 1)/2$, which neglects FSI and two–nucleon stimulated decay effects, sometimes used in experimental analyses. Even the naïf model of FSI proposed by Kim et al. in Ref. [5] is far from being supported by a detailed calculation.

Concerning nucleon–nucleon correlation observables, while there is fair agreement among our predictions and data in the case of N_{nn} , we overestimate the observations in the case of N_{np} . The origin of such a difference is likely the same as the one responsible for the mentioned disagreement on the single–proton spectra. Another indication supporting this possibility comes from the fact that we also overestimate the experimental distributions for N_{pp} . We have thus advanced the hypothesis that the experiment could have systematically underestimated the number of protons emitted in $^{12}\Lambda\text{C}$ decay, thus leading to the underestimation of N_p , N_{np} and N_{pp} spectra. On the contrary, for the observables involving only neutron detection, N_n and N_{nn} , theory and experiment turn out to agree. The same conclusion can be drawn in terms of the finite nucleus results. A clarification of the mentioned eventuality is desirable for an accurate determination of the Γ_n/Γ_p ratio.

Indeed, in this paper as well as in previous ones [14,15], Γ_n/Γ_p has been determined from data on N_{nn}/N_{np} . Here, for $^{12}\Lambda\text{C}$ we have obtained $\Gamma_n/\Gamma_p = 0.43 \pm 0.10$, whose central value could be lowered to about 0.3 if the measured neutron–proton distributions resembled those of our evaluations. The conclusion remains the same by using the finite nucleus analysis. The effect of the two–nucleon induced decay modes on the extracted Γ_n/Γ_p turn out to be small due to the restrictions imposed on angular and energy correlations. In any case, one has to bear in mind that ratios in the interval 0.3–0.5 would be compatible with most of today’s pure theoretical evaluations, which are also affected by uncertainties, especially due to the degree of arbitrariness in the experimentally unknown baryon couplings. These

models can also reproduce the observed total non-mesonic decay rates.

Before concluding, we want to make a brief comment on the two-nucleon induced mode. Because of the small or anyhow moderate dependence of the determined Γ_n/Γ_p values on these decay channels, triple coincidence measurements reveal to be necessary for the purpose of disentangling one- and two-nucleon stimulated decays in observed events.

To summarize, while we can safely assert that analyses of correlation measurements definitely solve the longstanding puzzle on the ratio Γ_n/Γ_p , single-nucleon spectra studies still provide ratios which are incompatible with what is obtained from pure theoretical models. We hope it will be possible to clarify soon the reasons of such a discrepancy.

ACKNOWLEDGMENTS

This work is partly supported by EURIDICE HPRN-CT-2002-00311, contract FIS2005-03142 from MEC (Spain) and FEDER, INFN-MEC collaboration agreement number 06-36, and Generalitat de Catalunya contract 2005SGR-00343. This research is part of the EU Integrated Infrastructure Initiative Hadron Physics Project under contract number RII3-CT-2004-506078.

REFERENCES

- [1] W. M. Alberico and G. Garbarino, Phys. Rep. **369**, 1 (2002); in *Hadron Physics*, IOS Press, Amsterdam, 2005, p. 125. Edited by T. Bressani, A. Filippi and U. Wiedner. Proceedings of the International School of Physics “Enrico Fermi”, Course CLVIII, Varenna (Italy), June 22 – July 2, 2004.
- [2] E. Oset and A. Ramos, Prog. Part. Nucl. Phys. **41**, 191–253 (1998).
- [3] O. Hashimoto et al., Phys. Rev. Lett. **88**, 042503 (2002).
- [4] Y. Sato et al., Phys. Rev. **C 71**, 025203 (2005).
- [5] J. H. Kim et al., Phys. Rev. **C 68**, 065201 (2003).
- [6] S. Okada et al., Phys. Lett. **B 597**, 249 (2004).
- [7] H. Bhang, in *DAPHNE 2004: Physics at meson factories*, Frascati Phys. Ser. **36**, 243 (2005). Edited by F. Anulli, M. Bertani, G. Capon, C. Curceanu–Petrascu, F. L. Fabbri and S. Miscetti.
- [8] H. Outa, in *Hadron Physics* (Ref. [1]) p. 219; H. Outa et al., Nucl. Phys. **A 754**, 157c (2005).
- [9] B. H. Kang et al., Phys. Rev. Lett. **96**, 062301 (2006).
- [10] M. J. Kim et al., nucl-ex/0601029.
- [11] M. Agnello et al., Nucl. Phys. **A 754**, 399c (2005); T. Bressani, E. Botta, A. Feliciello and V. Paticchio, Nucl. Phys. **A 754**, 410c (2005).
- [12] T. Nagae, Nucl. Phys. **A 754**, 443c (2005).
- [13] I. Tanihata et al., Hypernuclei with Stable Heavy Ion Beam and RI–beam Induced Reactions at GSI (HypHI), Letter of Intent, February 2005.
- [14] G. Garbarino, A. Parreño and A. Ramos, Phys. Rev. Lett. **91**, 112501 (2003).
- [15] G. Garbarino, A. Parreño and A. Ramos, Phys. Rev. **C 69**, 054603 (2004); W. M. Alberico, G. Garbarino, A. Parreño and A. Ramos, nucl-th/0407046, in *DAPHNE 2004: Physics at meson factories*, Frascati Phys. Ser. **36**, 249 (2005). Edited by F. Anulli, M. Bertani, G. Capon, C. Curceanu–Petrascu, F. L. Fabbri and S. Miscetti.
- [16] D. Jido, E. Oset and J. E. Palomar, Nucl. Phys. **A 694**, 525 (2001).
- [17] A. Parreño and A. Ramos, Phys. Rev. **C 65**, 015204 (2002); A. Parreño, A. Ramos and C. Bennhold, Phys. Rev. **C 56**, 339 (1997).
- [18] K. Itonaga, T. Ueda and T. Motoba, Phys. Rev. **C 65**, 034617 (2002).
- [19] E. Bauer and F. Krmpotić, Nucl. Phys. **A 717**, 217 (2003).
- [20] E. Bauer and F. Krmpotić, Nucl. Phys. **A 739**, 109 (2004).
- [21] S. Ajimura et al., Phys. Rev. Lett. **84**, 4052 (2000).
- [22] T. Maruta et al., nucl-ex/0509016; Nucl. Phys. **A 754**, 168c (2005).
- [23] W.M. Alberico, G. Garbarino, A. Parreño and A. Ramos, Phys. Rev. Lett. **94**, 082501 (2005).
- [24] C. Barbero, A. P. Galeão and F. Krmpotić, Phys. Rev. **C 72**, 035210 (2005); C. Barbero, C. De Conti, A. P. Galeão and F. Krmpotić, Nucl. Phys. **A 726**, 267 (2003).

- [25] K. Sasaki, M. Izaki, and M. Oka, Phys. Rev. **C 71**, 035502 (2005); K. Sasaki, T. Inoue and M. Oka, Nucl. Phys. **A 707**, 477 (2002).
- [26] A. Parreño, C. Bennhold and B.R. Holstein, Phys. Rev. **C 70**, 051601(R) (2004); Nucl. Phys. **A 754**, 127c (2005).
- [27] A. Montwill et al., Nucl. Phys. **A 234**, 413 (1974).
- [28] A. Sakaguchi et al., Phys. Rev. **C 43** (1991) 73.
- [29] J. J. Szymanski et al., Phys. Rev. **C 43**, 849 (1991).
- [30] H. Noumi et al., Phys. Rev. **C 52**, 2936 (1995).
- [31] H. Noumi et al., Proceedings of the *IV International Symposium on Weak and Electromagnetic Interactions in Nuclei*, edited by H. Ejiri, T. Kishimoto and T. Sato (World Scientific, Singapore, 1995), p. 550.
- [32] A. Ramos, M. J. Vicente-Vacas and E. Oset, Phys. Rev. **C 55**, 735 (1997); **66**, 039903(E) (2002).
- [33] A. Ramos, E. Oset and L. L. Salcedo, Phys. Rev. **C 50**, 2314 (1994).
- [34] W. M. Alberico, A. De Pace, G. Garbarino and A. Ramos, Phys. Rev. **C 61**, 044314 (2000).
- [35] E. Oset and L. L. Salcedo, Nucl. Phys. **A 443**, 704 (1985).
- [36] W. M. Alberico, A. De Pace, G. Garbarino, R. Cenni, Nucl. Phys. **A 668**, 113 (2000).
- [37] E. Bauer, A. Polls and A. Ramos, Phys. Rev. **C 58**, 1052 (1998).
- [38] W. M. Alberico, M. Ericson and A. Molinari, Ann. Phys. **C 154**, 356 (1984).
- [39] R. Machleidt, K. Holinde and Ch. Elster; Phys. Rep. **149**, 1 (1987).
- [40] M. B. Barbaro, A. De Pace, T. W. Donnelly and A. Molinari, Nucl. Phys. **A 596**, 553 (1996).
- [41] J. Cugnon and P. Henrotte, Eur. Phys. J. **A 16**, 393 (2003).